HHS Public Access

Author manuscript

Mol Psychiatry. Author manuscript; available in PMC 2024 April 24.

Published in final edited form as:

Mol Psychiatry. 2024 June ; 29(6): 1620–1635. doi:10.1038/s41380-022-01834-x.

Analyses of the autism-associated neuroligin-3 R451C mutation in human neurons reveal a gain-of-function synaptic mechanism

Le Wang[1,2,12], **Vincent R. Mirabella**[1,3,12], **Rujia Dai**[4], **Xiao Su**[1], **Ranjie Xu**[5], **Azadeh Jadali**[5], **Matteo Bernabucci**[1], **Ishnoor Singh**[1], **Yu Chen**[2], **Jianghua Tian**[2], **Peng Jiang**[5], **Kevin Y. Kwan**[5], **ChangHui Pak**[6], **Chunyu Liu**[2,4,7], **Davide Comoletti**[1,8], **Ronald P. Hart**[5], **Chao Chen**[2,9,10], **Thomas C. Südhof**[3,11], **Zhiping P. Pang**[1]

[1]Child Health Institute of New Jersey and Department of Neuroscience and Cell Biology, Robert Wood Johnson Medical School, Rutgers University, New Brunswick, NJ 08901, USA.

[2]Center for Medical Genetics & Hunan Key Laboratory of Medical Genetics, School of Life Sciences, and Department of Psychiatry, The Second Xiangya Hospital, Central South University, 410008 Changsha, China.

[3]Department of Molecular & Cellular Physiology, Stanford University School of Medicine, Stanford, CA 94305, USA.

[4]Department of Psychiatry, SUNY Upstate Medical University, Syracuse, NY 13210, USA.

[5]Department of Cell Biology and Neuroscience, Rutgers University, Piscataway, NJ 08854, USA.

[6]Department of Biochemistry & Molecular Biology, University of Massachusetts, Amherst, MA 01003, USA.

[7]School of Psychology, Shaanxi Normal University, 710000 Xi'an, Shaanxi, China.

[8]School of Biological Sciences, Victoria University of Wellington, Wellington 6012, New Zealand.

[9]National Clinical Research Center for Geriatric Disorders, Xiangya Hospital, Central South University, 410008 Changsha, Hunan, China.

[10]Hunan Key Laboratory of Animal Models for Human Diseases, Central South University, 410008 Changsha, Hunan, China.

[11]Howard Hughes Medical Institute, Stanford University School of Medicine, Stanford, CA 94305, USA.

Correspondence and requests for materials should be addressed to Chao Chen , Thomas C. Sudhof or Zhiping P. Pang, chenchao@sklmg.edu.cn; tcs1@stanford.edu; pangzh@rwjms.rutgers.edu.

AUTHOR CONTRIBUTIONS

LW conducted the experiments including cell culture, electrophysiology, morphological, cell transplantation and genomics analysis. VRM conducted the CRISPR/Cas9 gene targeting, related analyses, cloned the overexpression constructs and provided conceptual input on experimental design. RD, XS, RX, MB, IS, YC, and JT, conducted part of the analysis. RH conducted the single-cell analysis. KYK, PJ, DC, CP, TCS, CL, CC planned the experiments and analyzed the data. VRM, LW, DC, ZPP, and TCS conceived the project. TCS and ZPP wrote the paper with input from all authors.

COMPETING INTERESTS

The authors declare no competing interests.

Supplementary information The online version contains supplementary material available at https://doi.org/10.1038/s41380-022-01834-x.

[12]These authors contributed equally: Le Wang, Vincent R. Mirabella.

Abstract

Mutations in many synaptic genes are associated with autism spectrum disorders (ASD), suggesting that synaptic dysfunction is a key driver of ASD pathogenesis. Among these mutations, the R451C substitution in the *NLGN3* gene that encodes the postsynaptic adhesion molecule Neuroligin-3 is noteworthy because it was the first specific mutation linked to ASDs. In mice, the corresponding *Nlgn3* R451C-knockin mutation recapitulates social interaction deficits of ASD patients and produces synaptic abnormalities, but the impact of the *NLGN3* R451C mutation on human neurons has not been investigated. Here, we generated human knockin neurons with the *NLGN3* R451C and *NLGN3* null mutations. Strikingly, analyses of *NLGN3* R451C-mutant neurons revealed that the R451C mutation decreased *NLGN3* protein levels but enhanced the strength of excitatory synapses without affecting inhibitory synapses; meanwhile *NLGN3* knockout neurons showed reduction in excitatory synaptic strengths. Moreover, overexpression of NLGN3 R451C recapitulated the synaptic enhancement in human neurons. Notably, the augmentation of excitatory transmission was confirmed in vivo with human neurons transplanted into mouse forebrain. Using single-cell RNA-seq experiments with co-cultured excitatory and inhibitory *NLGN3* R451C-mutant neurons, we identified differentially expressed genes in relatively mature human neurons corresponding to synaptic gene expression networks. Moreover, gene ontology and enrichment analyses revealed convergent gene networks associated with ASDs and other mental disorders. Our findings suggest that the *NLGN3* R451C mutation induces a gain-of-function enhancement in excitatory synaptic transmission that may contribute to the pathophysiology of ASD.

INTRODUCTION

Autism spectrum disorders (ASD) are characterized by social interaction deficits, repetitive patterns of behavior, and language impairments and exhibit a 60–90% genetic heritability [1-4]. Altered neuronal connectivity and synaptic dysfunction are hypothesized to underlie the pathophysiology of ASD, similar to that of other neurodevelopmental disorders, including schizophrenia and intellectual disabilities [5]. Many genes encoding synaptic proteins were associated with ASDs and other neurodevelopmental disorders, including the genes encoding neuroligins (NLGNs) and neurexins (NRXNs), that are adhesion molecules which control the specification of synapse properties [6, 7].

The first gene mutation that was linked to ASDs was a mutation of the highly conserved arginine-451 to cysteine in the *NLGN3* gene (*NLGN3* R451C mutation) [8]. The functional impact of *NLGN3* R451C mutation has been intensely studied in heterologous expression systems [9-11] and in *Nlgn3* R451C-knockin mice [12, 13]. *Nlgn3* R451C-knockin mice showed that the R451C mutation diminishes surface trafficking of NLGN3 protein, resulting in decreased levels of NLGN3 [11, 13, 14]. Despite the reduction of *Nlgn3* expression in *Nlgn3* R451C-knockin mice, inhibitory synaptic transmission in the cortex [12], excitatory synaptic transmission in hippocampal pyramidal cells [13] and cerebellar Purkinje cells are enhanced [14]. *Nlgn3* R451C-knockin mice displayed impaired social interactions [12, 15], a core symptom of ASD, but surprisingly exhibited an increased spatial learning ability

[12] and enhanced repetitive behaviors [16]. Although another independently generated line of *Nlgn3* R451C-mutant mice revealed minimal aberrant behavioral phenotypes [17], both strains of mutant mice exhibited region-specific synaptic deficits [13]. However, none of the synaptic changes and behavioral abnormalities observed in *Nlgn3* R451C-mice were detected in *Nlgn3* knockout (KO) mice [12, 13]. These findings suggested a gain-of-function mechanism of the *NLGN3* R451C mutation that is likely cell type dependent [12, 18]. Indeed, paired recordings in the hippocampus revealed that the *Nlgn3* R451C mutation causes a gain-of-function phenotype in one type of synapse that is different from the *Nlgn3* KO, but a loss-of-function phenotype in another synapse due to decreased Nlgn3 protein levels that is the same as that of the *Nlgn3* KO [19]. Although this detailed information on the effect of the *Nlgn3* R451C mutation exists for mice, no data are available for the effect of the *NLGN3* R451C mutation in human neurons.

The development of efficient methods for generating neurons from human pluripotent stem cells [20-23] has provided an opportunity to use human neurons from modeling neuropsychiatric disorders [24-27]. Notably, mutations in the *NRXN1* [28, 29] and *NLGN4* [30, 31] genes in human neurons have uncovered intriguing functional changes that appear to be specific to human neurons. These studies provided important insights into how *NRXN1* and *NLGN4* mutations cause a synaptic dysfunction that could underlie the pathophysiology of ASD. However, no such information is available for the *NLGN3* R451C mutation. Therefore, we have now generated human embryonic stem (ES) cell lines with *NLGN3* R451C- and *NLGN3* null mutations, which enabled us to dissect the functional impact of the *NLGN3* R451C mutation in human neurons. Analyses of R451C-mutant excitatory and inhibitory human-induced neurons (iNs) revealed a reduction in NLGN3 expression, and an enhanced excitatory synaptic strength. This phenotype was not attributed to a decrease in NLGN3 expression because in *NLGN3* knockout human neurons, we detected a reduction in excitatory synaptic transmission. Overexpression of NLGN3 R451C but not the wild-type NLGN3 caused an augmentation in excitatory synaptic strengths. No significant cell death and endoplasmic reticulum (ER) stress were found to be associated with the R451C mutation. When R451C-mutant and control iNs were grafted into the mouse brain, a similar augmentation of excitatory synaptic transmission was observed in *NLGN3* R451C-mutant human iNs. Single-cell RNA-seq of co-cultured excitatory and inhibitory iNs revealed that the *NLGN3* R451C mutation causes differential expression gene (DEG) changes in excitatory neuronal gene networks related to synaptic transmission. These DEGs were found to be associated with ASD, schizophrenia, and bipolar disorders but unrelated to major depressive disorder and obesity. Our findings suggest that the *NLGN3* R451C mutation dramatically impacts excitatory synaptic transmission in human neurons, thereby triggering changes in overall network properties that may be related to mental disorders.

METHODS

Cell culture

Human H1 ES cells (WA01 WiCell Research Institute, Inc.) and one induced pluripotent stem (iPS) cell line (03SF) that we recently published [32] were cultured at 37 °C, 5% CO_2

on Matrigel® Matrix (Corning Life Sciences)-coated plates in mTeSR1 medium (Stem Cell Technologies) and maintained as described previously [32].

Animals

All animal work was performed without gender bias under the Institutional Animal Care and Use Committee (IACUC) protocol approved by Rutgers University IACUC Committee. *Rag2*$^{-/-}$ immunodeficient mice (JAX# 017708) were used for cell transplantation. Wild-type C57BL/6J mice at postnatal day 0–3 (P0–3) were used for glial culture [32]. Briefly, P0-P3 mouse cortices were digested with papain, 1 μM Ca^{2+}, 0.5 μM EDTA solution for 15 min at 37 °C. Glial cells were passaged twice to eliminate mouse neuron cells and cultured with 10% fetal bovine serum in DMEM (Invitrogen).

Gene targeting

R451C-mutant and NLGN3 KO ES cell lines were generated using CRISPR/Cas9 genome knockin and knockout (KO) [33]. Briefly, to target the *NLGN3* locus of the H1 ES cells, sgRNA designed from Optimized CRISPR Design Tool (http://crispr.mit.edu/), PX459 vector expressing Cas9 (Addgene #62988), and single-stranded oligodeoxynucleotide (ssODN) were transfected using the Lipofectamine 3000 reagent (ThermoFisher Scientific, L300015). The ssODN contained 140 base pairs of homology arms flanking the mutation site carrying mutations for R451C, a Mul1 restriction enzyme site for screening, along with a mutated PAM sequence. Individual clones were hand-picked for expansion and screening by PCR and sequencing. The two homozygous R451C knockin and two homozygous NLGN3 KO clones were further subcloned before expansion and freezing. Top 10 off-target genomic loci were confirmed by PCR and sanger sequencing analysis.

Lentiviral generation

Lentiviruses were produced as described [34, 35] in HEK 293FT cells (ATCC) by co-transfection with 3rd generation helper lentivirus plasmid (pMDLg/pRRE, VsVG and pRSV-REV) using calcium phosphate transfections. Lentiviral particles were collected in mTeSR1 medium, aliquoted, and stored at −80 °C. The following lentivirus constructs were used: (1) FUW-TetO-Ngn2-P2A-puromycin; (2) FUW-TetO-Ascl1-T2A-puromycin; (3) FUW-TetO-Dlx2-IRES-hygromycin; (4) FUW-rtTA; (5) FSW-L309-mCherry; (6) FSW-Venus; (7) FUW-L309-GFP; (8) FUW-NLGN3-HA; and (10) FUW-NLGN3 R451C-HA.

Generation of iN cell

Excitatory- (i.e. Ngn2-iNs) and inhibitory-human iNs (AD-iNs) were generated as described [36, 37]. Briefly, ESCs were dissociated by Accutase (Stem Cell Technologies) and plated in six-well plate coated with Matrigel® Matrix (Corning Life Sciences) and mTeSR1 containing RHO/ROCK pathway inhibitor Y-27632. At the same time of the plating, lentivirus cocktails prepared as described above (200 μl/well of six-well μlate) was added. On day 1, the culture medium was replaced with Neurobasal medium (Gibco) containing doxycycline (2 μg/ml), and doxycycline was maintained in the media for ~2 weeks. On days 2 and 3, infected cells were selected by puromycin and hygromycin (1 μg/ml). On day 4, mouse glia cells were plated on Matrigel-coated coverslips (5×10^4 cells/single well

of 24 well plates). On day 5, AD-iNs: Ngn2-iNs at 6:4 ratio (total of 2×10^5 cells/well) were mixed and plated on a monolayer of mouse glial cells. To differentiate excitatory- and inhibitory iN cells, cells were infected with lentivirus expressing either GFP or mCherry before co-culture. On Day 6, media change occurred using Neurobasal medium containing growth factors (BDNF, GDNF, NT3, all at 10 ng/ml), B27, and 1% GlutaMax. Cytosine β-D-arabinofuranoside (AraC, 2 μM) was added to the medium to stop glial cell division on day 3-4 after replating. For overexpression of NLGN3 and NLGN3 R451C, Ngn2-iNs were used. Lentiviral vectors control (GFP); NLGN3 or NLGN3 R451C were added together with Ngn2/rtTA viruses. Morphological, biochemical, and functional analyses were conducted after 5–6 weeks after replating. Each of the morphological and functional analyses was conducted from at least three independent culture batches. These included multiple batches of cultures of H1 ESC in different culture wells, and all data were pooled together.

Cell transplantation

R451C-mutant (labeled by mVenus) and wild-type (labeled with mCherry) Ngn2-iNs (14 days after induction) were dissociated and mixed at 1:1 ratio (1×10^5 cells per μl in PBS). As described previously [38, 39], the cells were then stereotaxically (ML: ±1.0 mm, AP: −2.0 mm, and DV −1.2 and −1.5 mm) injected into the cortex and hippocampus of P0 to P3 $Rag^{2-/-}$ immunodeficient mice. The pups were weaned at P21 and were kept up to 6 weeks before characterization. All recordings been done from both the control and the R451C iN cells were done from the same areas. We did not observe any tumor formation of the transplanted cells in any of the animals.

Immunofluorescence experiments and analysis

Primary antibodies were diluted in blocking buffer (1% goat serum, 0.25% Triton X-100 and 4% BSA) at 4 °C and incubated overnight. Cultures were washed 3 times with blocking buffer and then incubated with secondary antibody (1: 500) at RT for 1 h. Following 3× DPBS washes, coverslips were mounted onto glass microscope slides with mounting medium containing DAPI. The following antibodies were used: Oct4 (Millipore Sigma MAB4401, 1:2000), Tra-1-60 (Millipore Sigma MAB4360, 1:1000), Map2 (Abcam, AB5392, 1:1000), Synapsin (Rabbit, 1:3,000, E028), VGAT (Millipore Sigma AB5062P, 1:500), Calnexin (Enzo ADI-SPA-860-D, 1:200), Calreticulin (Enzo ADI-SPA-600-D, 1:200) and Caspase-3 (Cell Signaling #9661, 1:200). At least three independent culture batches were used for all experiments.

Synaptic puncta density analysis.—Immunofluorescence was performed on iNs at day 40–50 with dendrite marker MAP2 and synaptic markers Synapsin-1 and VGAT. Confocal images were taken using a Zeiss LSM700 laser-scanning confocal microscope with a 63× objective. All images were acquired using Z stack maximal projection in Zeiss Zen blue software. Correlated synaptic puncta size and intensity were quantified by *Intellicount* as reported previously [40]. Puncta density and primary processes were blindly counted and quantified.

ER structure analysis.—Immunofluorescence was performed on iNs at day 42 with dendrite marker MAP2, and ER markers Calnexin and Calreticulin. Images of iNs were

obtained as z-projections on a Zeiss LSM700 laser-scanning confocal microscope using a 63x objective. Confocal images were analyzed by ImageJ [41], as reported previously [42]. Using the line tool of ImageJ, a 10 μm line was drawn from the nuclear envelope towards the periphery of each cell analyzed. Intensity and coefficient variation (C.V.) was calculated all along the 10 μm line. iN soma ER area and intensity was calculated by using the Image J ROI tool and normalized with MAP2.

Western blot analysis

For induced neuron culture, at day 40–50, the cultures were washed once with PBS. The proteins were directly collected by 2× SDS loading buffer (4% SDS, 125 mM Tris Hcl (pH, 6.8), 20% glycerol, 5% 2-mercaptoethanol and 0.01% bromophenol blue) [43]. Protein samples then were denatured by heating to 95 °C for 5 min. The denatured protein samples were allowed to cool down and equal amounts of samples (30 μl) were analyzed by 4–15% TGX gels (Biorad # 4561084DC) for sequential Western blots on the same membranes. The protein from the gel was then transferred to a 0.45 μm nitrocellulose membrane (Biorad #1620115) using the BIO-RAD transferring system. Nitrocellulose membrane was blocked in 5% nonfat milk for 1 h at room temperature. After the blocking step, membranes were incubated with primary antibody overnight at 4 °C. The following day, the blots were washed three times with Tris-buffered saline with 0.1% Tween 20 (TBST) before the addition of horseradish peroxidase-conjugated secondary antibody at room temperature for 1 h. All ER stress-related proteins referred to here were purchased from Cell Signaling Technology as an ER Stress Antibody Sampler Kit (CST, #9956, all 1:1000). Rabbit Nlgn3 (RRID: AB_2571813, Frontiers Institute, Japan, 1:1000) [44], Rabbit Syntaxin (I378, Sudhof laboratory, 1:5000). Protein bands were visualized by the addition of Clarity Western ECL Substrate (Biorad # 1705060). The density of the bands was quantified using ImageJ software. Beta-actin was measured as a loading control.

Gene expression analyses

Total neuronal RNA from three independently generated batches of cultures were prepared using TRIzol ® Reagent (Thermo Fisher Scientific). Human-specific primers were used for *NLGN3, MAP2, Tuj1, VGAT, Vglut1, Vglut2, GABBR1, ACTB*, and PCR reaction conditions followed the manufacturer's recommendations. Student's *t*-test was used to compare grouped control and R451C means. Evaluation of qPCR was performed blind to the genotype. See Supplementary Table 2 for a complete list of human-specific primers used in this study.

Electrophysiology

Cell culture electrophysiology.—Whole-cell patch-clamp electrophysiology for co-cultured iN cells was performed as described [32]. For spontaneous postsynaptic current and current-clamp recordings, K-gluconate internal solution was used, which consisted of (in mM): 126 K-gluconate, 4 KCl, 10 HEPES, 0.05 EGTA, 4 ATP-magnesium, 0.3 GTP-sodium, and 10 phospho-creatine. Spontaneous postsynaptic currents were recorded at a holding potential of −70 mV. Inhibitory postsynaptic currents (IPSCs) were pharmacologically isolated in the presence of 20 μM CNQX; and excitatory postsynaptic

currents (EPSCs) were recorded in the presence of 50 μM picrotoxin (PTX). Miniature postsynaptic currents were recorded at a holding potential of −70 mV in the presence of 1 μM tetrodotoxin (TTX) with 20 μM CNQX (for mIPSCs) or 50 μM PTX (for mEPSCs). For miniature postsynaptic current recording, Cs-based solution was used, which consisted of (in mM): 40 CsCl, 3.5 KCl, 10 HEPES, 0.05 EGTA, 90 K-gluconate, 1.8 NaCl, 1.7 $MgCl_2$, 2 ATP-magnesium, 0.4 GTP-sodium, and 10 phosphocreatine. The recording external solution contained (in mM): 140 NaCl, 5 KCl, 10 HEPES, 2 $CaCl_2$, 2 $MgCl_2$, 10 Glucose, pH 7.4. All cell culture recordings were conducted at room temperature.

Brain slice recording.—Mice were anesthetized and brains were quickly removed into ice-cold oxygenated artificial cerebrospinal fluid (ACSF) cutting solution (in mM): 50 sucrose, 2.5 KCl, 0.625 $CaCl_2$, 1.2 $MgCl_2$, 1.25 NaH_2PO_4, 25 $NaHCO_3$, and 2.5 glucose). Coronal section slices at 300 μm were cut using a vibratome (VT 1200 S; Leica). After 1 h recovery (33 °C) in ACSF (in mM)125 NaCl, 2.5 KCl, 2.5 $CaCl_2$, 1.2 $MgCl_2$, 1.25 NaH_2PO_4, 25 $NaHCO_3$, and 2.5 glucose, slices were transferred to a recording chamber and perfused with ACSF at 30 °C. Whole-cell patch-clamp recordings were performed as described [45]. For electrophysiological recordings of evoked EPSCs, the stimulation electrodes were placed 100–150 μm lateral to the recording sites as described [46].

Cells were excluded from analysis if series resistance (Rs) changed by more than 20% during the recording. In addition, any recordings where the access resistance was greater than 25 MΩ were also excluded from the analysis. Electrophysiological data were collected by pClamp 10.5 (Molecular Devices) using MultiClamp 700B (Molecular Devices). Spontaneous EPSCs (sEPSCs), spontaneous IPSCs (sIPSCs), miniature EPSCs (mEPSCs) and miniature IPSCs (mIPSCs) were detected using template search algorithm for event detection in Clampfit 10.5 (Molecular Devices). The cumulative plots of the distributions of spontaneous and miniature synaptic releases consist of the averages of all cells recorded under each condition.

Visualization of the targeting gene expression

To visualize the spatiotemporal expression of the *NLGN1, NLGN2, NLGN3, NLGN4X*, and *NLGN4Y* in the human brain, we used the median value of these genes as the signature value to visualize in the GTEx v8 data and BrainSpan data. This analysis was performed using cerebroViz R package [https://github.com/ethanbahl/cerebroViz] [47]. We also tested the expression of *NLGN3* in the single-cell data of ASD and visualized with heatmap using ggplot2 R package. All analysis was performed in R v3.6.

Single-cell RNA-seq analyses

For control and two R451C subclones, two wells of a six-well plate were plated with mixed cultures at 2×10^6 iNs and 2.5×10^5 glia/well. On day 40, cells were dissociated with TrypLE (Thermo Fisher) for 5 min at 37 °C, which preferentially releases neurons from glia. The dissociated cells were centrifuged at 200 × *g* for 5 min at 4°C, and cells were washed twice with 1× HBSS (Thermo Fisher), resuspended at 1200 cells/μl in 1% Bovine Serum Albumin (BSA)/1× PBS and placed on ice. Single-cell cDNA libraries were generated using the Chromium Next GEM Single-Cell 3’ GEM Reagent Kits v3.1 (10X Genomics).

Approximately 2×10^4 dissociated cells were loaded onto a cassette in the Chromium Controller with accompanying reagents to generate Gel Beads in Emulsions (GEMs). These were reverse transcribed to single-cell cDNA libraries before the oil emulsion was disrupted and cDNA was purified using Dynabeads MyOne Silane (Thermo Fisher). cDNA was amplified by PCR for 11 cycles and purified using SPRIselect reagent (Beckman–Coulter). cDNA fragmentation, A-tailing, and end repair was performed followed by adapter ligation for paired-end sequencing. An additional 12 cycles of PCR were performed to incorporate the sample index sequences and to amplify the libraries before purification and sequencing. Single-cell RNA-seq libraries were sequenced by Psomagen® using the Illumina Novaseq platform.

Raw reads were aligned with pooled mouse (mm10) and human (GRCh38) reference genomes and pre-processed using Cellranger software (v.4.0.0, 10X Genomics). Analysis of reads mapped per cell identified >90% human cells, <10% cell mouse cells. After loading cell × gene data into R using the Seurat (v. 4.0.2) package [48, 49], only cells expressing human genes were isolated for further analysis. After filtering (number of features between 200 and 10,000 per cell, less than 10% mitochondrial RNA), normalization, scaling, and PCA projection, the UMAP (Uniform Manifold Approximation and Projection) coordinates were calculated, and graph-based clustering was performed. In order to further determine the cell identity of our iNs in the co-culture, we reassigned and compared each cell type to the developing human fetal brain cell types by using human cortex fetal brain maker genes [50]. Specifically, we applied ScType [51] on cell type assignment and clustering. Average log fold change gene expression of each cell type was used for PCA projection.

Differentially expressed genes (DEG) expression analysis was performed by applying a Mann–Whitney U test on three relatively most mature cell clusters (excitatory, GABA1, and GABA2 inhibitory neuron), comparing combined R451C samples with control. P values were adjusted by Benjamini–Hochberg to a false discovery rate (q value). All graphs and analyses were generated and performed in R.

ScType analysis

To identify cell types in our scRNAseq results, we used the R function sc_type() from ScType [51]. Genes specific for human fetal brain cell types were obtained from either Polioudakis et al. [52] or Nowakowski et al. [50]. In both cases, up to 25 genes with the highest $\log_2$ fold change (selected clusters vs. all other clusters) were selected for each cell type. Results were plotted, comparing our original UMAP cell type identification with bubble plots, showing strengths of matching to known cell types by bubble area and re-labeled UMAP plots, showing the best matches from each dataset. A principal components plot compared reduced dimensionality of $\log_2$ fold-changes for our clusters compared with the cell types defined by the Nowakowski comparison dataset [50].

Analyses of genomic integrity using e-Karyotyping analysis

The e-Karyotyping analysis was performed as described [53]. Briefly, the single-cell RNA-seq data were merged as pseudobulk RNAseq reads, and the GATK HaplotypeCaller program were used to call SNPs [54]. Next, we filtered out SNPs below a threshold coverage

of 20 reads, and SNPs with a frequency below 0.2 of the less-expressed allele. Allelic ratio graphs and analyses were generated and performed in R as described previously [53].

SynGo annotation

For analysis of DEGs associated with synaptic function, GO analysis was performed using the SynGO [55] website: https://www.syngoportal.org/.

Cell–cell communication analysis

Cell communication analysis was conducted in the CellChat package (version 0.0.1) [56]. The library-size normalized scRNA-seq data were loaded into CellChat. The human ligand-receptor pairs in the database CellChatDB were used for calculating the cell interactions. The main steps for constructing cell–cell communication networks are as follows: (1) identifying overexpressed ligand or receptors in one cell type and their interactions based on scRNA-seq data, (2) calculating the probability of cell interactions at the ligand-receptor pair level, and 3) inferring the cell communication probability at the signal pathway level. Networks were constructed in the control cell line and R451C cell line separately. The comparison of the total number of interactions and strength (probability of interaction) between two cell lines was conducted with the function *compareInteractions*. Mann–Whitney *U* test was used to compare the strength of interactions mediated by pathways *NRXN* and *NEGR*.

Protein-protein interaction (PPI) network construction

The Search Tool for the Retrieval of Interacting Genes/Proteins database (STRING v11.0) [57] was used to construct PPI network. Given gene NLGN3 (protein NLGN3) and the lists of differentially expressed genes in GABA1 neurons, GABA2 neurons, and excitatory neurons (adjusted p value<0.05), STRING can search the proteins that have interactions with NLGN3 and construct subnetworks. K-means was used for network clustering. The genes connected to NLGN3 were defined as NLGN3-PPI-genes.

Overrepresentation analysis of psychiatric disorder-related genes

To explore whether DEGs may be part of the same network or pathway as known susceptibility genes of psychiatric disorders, we tested for enrichment between DEGs and disorder-associated genes. Fisher's exact test was used in the enrichment test. Significance was assessed using Fisher's exact test, followed by FDR correction of p values and OR > 1. We collected the genes from multiple resources which were classified into 46 categories. The gene identifiers were converted to Ensembl Gene IDs in Gencode (version v19 hg19).

Quantification and statistical analysis

All data are presented as the mean ± standard error of the mean (SEM), unless otherwise noted. All experiments were repeated on at least three biological replicates, with each replicate consisting of an independent infection/differentiation. Statistical significance (**p <0.01; ***p < 0.001) was evaluated with the Kolmogorov–Smirnov-test (for cumulative probability plots), one-way ANOVA and Student's t-test (for bar-graph).

RESULTS

NLGN3 R451C mutation affects excitatory synapse formation and increases the strength of excitatory synaptic transmission

We first examined the expression of *NLGN3* in the human brain by evaluating the region-wide expression of *NLGN* genes (*NLGN1-4Y*) in the brain using the Genotype-Tissue Expression (GTEx) database [58]. *NLGN2* and *NLGN3* are both abundantly expressed in the human frontal lobe (FL) and cerebellum (CB) (Supplementary Fig. 1a & b). Using the BrainSpan human brain development database [59], we found that *NLGN3* is present at high levels during late prenatal and early postnatal development (Supplementary Fig. 1c, d). Consistent with current ASD de novo variant genetic findings, ASD risk genes related to synaptic communication are highly expressed in the brain at perinatal stages and have unique expression patterns compared with other groups of risk genes [60]. *NLGN* genes are expressed in both glia and neurons [61, 62]. To verify the cell type-specific expression of *NLGN3* in the human brain, we examined the ASD patient single-cell dataset [63] and found that the *NLGN3* gene is expressed in both neuronal (GABA and glutamate neurons) and glial cells (Supplementary Fig. 1e). Although the gene expression data thus suggest that *NLGN3* may have a function in both neurons and in glia, we decided to focus here on neurons because the goal of the current study was to determine whether the well-documented role of Nlgns in murine synapses [6, 64, 65] also applies to human neurons.

To study the potential role of the *NLGN3* R451C mutation in human neurons, we used CRISPR-Cas9 to introduce the R451C mutation into well-characterized human H1 embryonic stem (ES) cells (Fig. 1a, b), which have been used to model mental disorders-related gene mutations, including *NRXN1* and *SHANK3* mutations [24, 29], in human neural context. We selected two subclones (clone A&B) and used the parental ES cell line at a similar passage number as wild-type (WT) control for morphological, biochemical, functional, and genomic analyses. Note that since the *NLGN3* gene is X-linked and H1 cells are male, only a single allele needs to be mutated. We confirmed the pluripotency of NGLN3 R451C-mutant ES cells by staining the cells for the stem-cell markers Tra-1-60 and OCT4 (Fig. 1c). Genomic integrity was confirmed using e-Karyotyping [53], which detected no apparent anomalies (Supplementary Fig. 2) and additionally excluded off-target mutations by sequencing the genomic DNA at the top predicted CRISPR off-target sites (Supplementary Table 1).

Using our well-characterized iN cell technology [35], we converted human control and *NLGN3* R451C-mutant ES cells into excitatory (with Ngn2) and inhibitory (with Ascl1 and Dlx2) neurons [35-37] (Fig. 1d). After induction, we co-cultured the two types of neurons and performed protein and gene expression analyses. Consistent with what was found in the mouse model of the *Nlgn3* R451C mutation [12], we observed that the R451C substitution caused a significant decrease in *Nlgn3* protein levels (~40% of control levels) but not in the expression levels of an unrelated synaptic vesicle marker Syntaxin-1 (Fig. 1e). The *NLGN3* mRNA levels, however, were not changed by the R451C knockin mutation as determined by quantitative RT-PCR (Supplementary Fig. 3a). These data suggest that the *NLGN3* R451C

mutation destabilizes the *NLGN3* protein, consistent with previous studies on the mutant protein in knockin rodent model [9-13].

To investigate whether *NLGN3* R451C-mutant neurons exhibit functional impairments of neuronal properties, we next performed whole-cell patch-clamp electrophysiology and morphological measurements. We found that *NLGN3* R451C-mutant neurons have intrinsic membrane properties and fire action potentials in response to current injections similar to control neurons (Fig. 1f, 2c-e). We further conducted comprehensive analyses on membrane properties, including whole-cell current responses and parameters of the action potentials in both control and *NLGN3* R451C-mutant human neurons. We found that in multiple parameters tested, including the rheobase, action potentials amplitude, half-width, threshold, after-hyperpolarization potentials (AHPs), sodium and potassium currents, the human neurons carrying *NLGN3* R451C mutation did not show significant differences when compared to controls (Fig. 1g-p). These data suggest that *NLGN3* R451C mutation likely does not affect the passive and active membrane properties in human neurons. However, neurons derived from both R451C-mutant cell lines exhibited a significant increase in the density of presynaptic Synapsin-positive puncta, suggesting an increased synaptic density. In contrast, the density of inhibitory vGAT-positive synaptic puncta was not changed, indicating that only excitatory synapse numbers are increased (Fig. 1q-t). Moreover, the number of primary dendritic processes showed no significant changes (Fig. 1u), suggesting that the R451C mutation does not affect dendritogenesis.

Next, we investigated synaptic transmission using the co-cultured excitatory and inhibitory neurons (Fig. 2a). We simultaneously recorded spontaneous excitatory (sEPSCs) and inhibitory postsynaptic currents (sIPSCs) from *NLGN3* R451C-mutant and control neurons and distinguished sEPSCs and sIPSCs based on their distinct kinetics [66] (Fig. 2b). These data suggested that co-cultured excitatory- (Ngn2-iNs) and inhibitory- (Ascl1 and Dlx2) neurons form complex functional networks. To quantify the changes in both excitatory and inhibitory synaptic transmission unambiguously, we used pharmacological isolation for the recordings of sEPSCs and sIPSCs in excitatory human neurons (labeled by expression of fluorescent proteins exclusive to Ngn2 iNs) in the presence of PTX or CNQX, respectively. The *NLGN3* R451C-mutant neurons exhibited a large (~3-fold) increase in the frequency, but not the amplitude, of sEPSCs without significant changes in sIPSCs (Supplementary Fig. 3b-e). In the presence of tetrodotoxin (TTX), which isolates action potential-independent but calcium-dependent single vesicular release, we detected a similar increase in miniature excitatory postsynaptic currents (mEPSCs) but not in miniature inhibitory postsynaptic currents (mIPSCs) in *NLGN3* R451C-mutant neurons compared to controls (Fig. 2f-i). Together, these results suggest that in human neurons, the *NLGN3* R451C mutation enhances the strength of excitatory but not inhibitory transmission at least in part by increasing synapse numbers.

Even though the reduction in the protein expression of NLGN3 was observed in the human neurons carrying the R451C mutation, we found a stronger excitatory synaptic release phenotype compared to the wild-type controls, suggesting that *NLGN3* R451C may cause a “gain-of-function” in excitatory synapses. To validate this, we set out to test whether the “gain-of-function” was a result of R451C substitution or rather due to decreased expression

of NLGN3. We used CRISPR-Cas9 strategy to generate two *NLGN3* knockout (KO) pluripotent stem cell lines using H1 ES cells (Supplementary Fig. 4a). PCR and Sanger sequencing showed that the two cell lines bear two different premature early stop codons at amino acids positions of 469 or 460 within exon 7 (Supplementary Fig. 4b). We confirmed the pluripotency of NGLN3 KO stem cells by using stem-cell markers Tra-1-60 and OCT4 (Supplementary Fig. 4c). Using Ngn2 approach, we rapidly generated excitatory neurons and co-cultured them on a monolayer mouse astrocytes (Fig. 2j). Western blots showed that NLGN3 protein expression was abolished in NLGN3 KO human neurons derived from the two KO cell lines (Fig. 2k). Using whole-cell patch-clamp recordings, we found a significant reduction (~50%) in the frequency of mEPSCs but not in the amplitude in the *NLGN3* KO iNs (Fig. 2l, m). Morphological analysis revealed no statistical changes in synapse numbers in NLGN3 KO compared to control (Supplementary Fig. 4d). To further validate the gain-of-function of *NLGN3* R451C mutation in human neurons, we next overexpressed wild-type NLGN3 and NLGN3 R451C constructs in a single control ES cell line and in a single unrelated control iPS cell line (Fig. 2n, o). Similar to the R451C knockin human neurons, we found an increase in mEPSC frequency in human neurons overexpressed with the R451C NLGN3 (Fig. 2p-s). These results indicate that *NLGN3* plays a role in regulating the synaptic strength of excitatory synapses in human neurons, and the “gain-of-function” phenotype in the R451C human neurons was not due to the reduction in the NLGN3 protein expression level.

The *NLGN3* R451C mutation is unlikely to cause endoplasmic reticulum (ER) stress

The R451C mutation decreases the level of *NLGN3* protein without lowering the expression of the NLGN3 mRNA in human neurons (Fig. 1e, Supplementary Fig. 3a), similar to observations made in *Nlgn3* R451C-mutant knockin mouse line [12]. These observations prompted the hypothesis that the *NLGN3* R451C mutation might impair neuronal function by inducing an ER stress response [14, 67]. Although it seems unlikely that ER stress would cause an increase in the number and strength of excitatory synapses, at least in the rodent cerebellar Purkinje cells it was suggested that an unfolded protein response (UPR) could enhance excitatory synaptic transmission [14]. These findings prompted us to investigate whether there exist *NLGN3* R451C mutation-induced ER stress or cell death in human neurons.

We first examined the morphology of the ER in human neurons. Staining of control and *NLGN3* R451C-mutant neurons showed that the signal of the ER marker calnexin did not show significant changes. The calreticulin signal exhibited an increase in neurons derived from one but not from the other of the two *NLGN3* R451C-mutant ES cell clones that we analyzed (Fig. 3a-l). Moreover, quantitative immunoblotting of major ER stress markers, including Calnexin, Ero1-Lα, IRE1α, PDI, and PERK, did not uncover consistent changes in the expression of these markers (Fig. 3m, n). Finally, we probed the neurons for evidence of cell death. Though certain trends were apparent, we detected no significant changes in the total number of neurons or the number of neurons that were stained by the apoptosis marker Caspase-3 (Fig. 3o, p). Together, these results suggest that the *NLGN3* R451C mutation does not cause a major impairment of neurons by ER stress, although a low level of ER stress activation cannot be ruled out.

The *NLGN3* R451C mutation increases excitatory synaptic connectivity of human neurons transplanted into mouse brain

Cultured neurons lack a physiologically relevant environment. Grafting of human neurons into rodent brains has been used to study human neuronal development and functionality [26, 38]. We transplanted control and NLGN3 R451C-mutant excitatory human neurons expressing mCherry (control) and mVenus (R451C mutant), respectively, simultaneously into the hippocampal region of neonatal (postnatal day 1) $Rag2^{-/-}$ immunocompromised mice (Fig. 4a) and analyzed the neurons 6 weeks later by imaging and electrophysiology. Human iNs were found to be located mainly at the injection sites and exhibited extensive branching around these sites (Fig. 4b, c).

We performed whole-cell patch-clamp recordings from mCherry-positive (control iNs) and mVenus-positive neurons (NLGN3 R451C-mutant iNs) in the same brain regions (both hippocampal and surrounding cortical regions) to control for confounding viabilities, such as inter-animal differences caused by the transplantation procedure. The transplanted human iNs received both excitatory and inhibitory synaptic inputs (Fig. 4d), suggesting that the grafted human neurons were functionally integrated into existing in vivo neuronal networks. As usual in such experiments, the integration of the transplanted neurons was only examined postsynaptically, which is appropriate since *NLGN3* is a postsynaptic protein. Similar to the findings in cultured neurons (Fig. 3), *NLGN3* R451C-mutant neurons derived from both ES cell clones exhibited a similar increase in the frequency but not in the amplitude of sEPSCs (Fig. 4e, f). Consistent with the increase in sEPSC frequency, we observed a large increase in evoked EPSC amplitude (stimulation electrodes were placed 100–150 μm laterally) in *NLGN3* R451C-mutant neurons compared to controls (Fig. 4g). We did not find any significant differences between R451C and control neurons in sIPSC frequency or amplitude, with a a strong trend towards an increase in frequency (Fig. 4i). These results confirm that the *NLGN3* R451C mutation enhances excitatory synaptic inputs in human neurons also in an in vivo paradigm, consistent with a gain-of-function phenotype. Note that we did not examine potential differences in synaptic phenotype between a hippocampal and cortical environment, which were identified murine *Nlgn3* R451C models.

The *NLGN3* R451C mutation is associated with distinct gene expression profiles in excitatory and inhibitory neurons

To gain insight into the underlying molecular mechanism of R451C *NLGN3* in human neurons and the observed synaptic phenotypes, we conducted single-cell RNA sequencing (sc-RNAseq) experiments in mixed cultures of excitatory or inhibitory neurons derived from control or *NLGN3* R451C-mutant ES cells (Fig. 5a). A total of 27,724 cells of high quality and sequencing depth were obtained (average number of genes/cells 3,995; the average number of reads 17,574) (Supplementary Fig. 5). Cluster identities were estimated using the top cluster-enriched genes. Despite the relatively homogenous human neuronal populations expected from using iN technologies [35-37], gene expression profiles corresponding to seven cell types were identified: (1) Relatively mature excitatory neurons (*GAP43, DCX, MAP2, NEFM, VMAP2, NSG1, NCAM1, SYT1, STMN2*); (2) relatively mature GABA1 inhibitory neurons (*TAC1, NTNG1, NTS, CALB1, NOS1, NPY, GAD2, GAL*), (3) GABA2 inhibitory neuronal cells (*NNAT, SSTR2, CNTN2*); (4) transitional excitatory neurons (*NES,*

DCX, KCNQ1OT1, CACNA1A, SCN3A, MAP6, NTM, NRXN1, NEFM, NNAT, KCNJ6, NEUROD1, NEUROD4, HOMER3, SLC17A7); (5) transitional inhibitory neurons (*VIM, NES, DLX5, DLX2, DLX1, GAD2*) and (6) intermediate neurons (*ASCL1, SOX2, NES, MKI67, LIX1, DCX, TAC1, GAP43, VAMP2, TOP2A, DCN, NTRK2, CENPF, ID3, TOP2A, PEA15, ID1, HES5*); and (7) neuronal progenitor cells (*SOX2, NES, POU5F1, CENPF, MKI67*) (Fig. 5b, Supplementary Figs. 6, 7 and Supplementary Table 3). Note that the transitional neuronal groups are likely representing those cells that failed to become fully reprogrammed, as found in previous reports [68, 69]. The distributions of the seven major cell types were reasonably consistent among neurons derived from control ES cells and the two clones of *NLGN3* R451C-mutant ES cells (Supplementary Fig. 8a, b). Due to the small sample size of the sc-RNAseq dataset generated, cell proportion analysis could not be accurately performed. Because NLGN3 is a synaptic adhesion molecule that was studied extensively in mouse models and heterologous systems [6], and there are no gross differences in our morphological analysis (Figs. 1 and 3), it is unlikely that R451C will affect neurodifferentiation in an iN cell model. We observed the expression of genes that characterize the human cortical layers I-V (*RELN*, Layer I; *CUX1, POU3F2*, layer II-III; *NECAB1*, layer IV and *BCL11B*, layer V) in induced human iNs, suggesting a phenotype reminiscent of cortical identity (Fig. 5c) [36, 37]. It has been shown that at transcriptional and chromatin accessibility levels, these induced excitatory glutamatergic and inhibitory GABAergic neurons are overall similar to fetal brain profiles [70]. We directly compared the iN cell transcriptome to that obtained from human fetal brain prefrontal cortex (PFC) and visual cortex (V1), which revealed that the iN cell clusters are in general similar to, but do not overlap those observed in human fetal cortex (Supplementary Fig. 9).

To investigate the potential impact of the *NLGN3* R451C mutation on synaptic gene expression, we limited our analysis to the relatively mature excitatory cluster and the inhibitory clusters (both GABA1 and GABA2). We examined the differentially expressed genes (DEGs; false discovery rate (FDR) < 0.05 and $\log_2$ fold change [log2FC] > 0.25) within individual clusters, comparing *NLGN3* R451C-mutant and control iNs (Supplementary Table 4). We identified 443 genes as DEGs in the excitatory cluster, 387 DEGs in the GABA1 inhibitory cluster, and 938 DEGs in the GABA2 cluster. Interestingly, these DEGs were mostly unique to the selected neuronal subtypes (26.5–1.9% overlaps), suggesting that the *NLGN3* R451C mutation may elicit distinct gene expression patterns in different types of neurons (Fig. 5d). For example, the ASD-related gene *FXR1* is upregulated in *NLGN3* R451C-mutant excitatory neurons (adjusted $P = 2.95 \times 10^{-58}$) and GABA1 inhibitory neurons (adjusted $P = 2.75 \times 10^{-18}$), but not in GABA2 inhibitory neurons.

We subsequently applied SynGo functional enrichment in all three neuronal subtype clusters using isolated upregulated and downregulated gene sets [55]. We found three groups of upregulated genes that are enriched in genes related to pre- and postsynaptic function categories. However, the excitatory neuron cluster exhibited a stronger enrichment in the downregulated synapse-related genes, especially those pertaining to postsynaptic functions (Fig. 5e). These functional annotations are consistent with the idea that the *NLGN3* R451C mutation induces heterogeneous gene expression changes in different neuronal cell types. The excitatory neuronal show more profound DEGs that are associated with synaptic

transmission, for example, synaptic vesicle exocytosis genes *VAMP2, SV2A, ATP6V0C, ATP6V0A1* are consistently upregulated in R451C *NGLN3* excitatory neurons but not in inhibitory neurons (Supplementary Table S5). These results suggest that *NLGN3* R451C mutation may have a more profound impact on excitatory synaptic transmission, consistent with our observations using in vitro and in vivo human neuronal models.

To further investigate the possible physical interactions that exist between NLGN3 and proteins encoded from the identified DEGs, a protein-protein interactions (PPIs) network associated with *NLGN3* was constructed with *NLGN3* and DEGs identified in three neuronal clusters (excitatory neurons, GABA1, and GABA2 inhibitory neurons). The first- and second-level neighbors to *NLGN3* were shown in Supplementary Fig. 11. Notably, we found a correlation between the *NLGN3* R451C mutation and CASK expression. CASK is a cytoplasmic scaffolding protein that interacts with presynaptic neurexins that bind to *NLGN3*, and human mutations in the *CASK* gene are also associated with ASDs [71-74]. *CASK* protein levels but not RNA expression is increased by a heterozygous conditional *NRXN1* deletion of human neurons, which exhibit a decrease in excitatory synaptic strength [29]. *Cask* deletion in mice, conversely, results in an increased mESPC frequency in cortical neurons [75].

To determine whether *NLGN3* affects the overall number/strength of the connection between neurons, we performed cell–cell interaction analysis in the R451C dataset and control dataset using CellChat [56]. We calculated the cell–cell interaction based on the expression of known ligands and receptors in cell clusters. Interestingly, we found an overall increase in cell–cell interaction number and strength in R451C neurons compared to the control dataset (Supplementary Fig. 10a, b). To identify the molecular pathways mediating the specific increase in interaction, we aggregated the interactions of ligand-receptor pairs by pathways. In the excitatory neuronal cluster, we found a significant increase in the interaction between NLGN3 and its presynaptic binding partner NRXN1 (but note that NRXN1 expression level was not significantly increased in the R451C neurons from sc-RNAseq result), as well as cell adhesion-related *NEGR* that may enhance synaptic function (Supplementary Fig. 10c) [7]. Thus, the concerted increase in the interaction between these ligand-receptor binding pairs in R451C excitatory neurons again strongly suggests a role for R451C function in enhancing synaptic transmission.

Finally, to further determine whether the DEGs associated with the *NLGN3* R451C mutation are related to neuropsychiatric disorders such as ASD, schizophrenia (SCZ), bipolar disorder (BP), and major depression disorder (MDD), we performed an enrichment test in the risk genes of ASD, SCZ, BP, and MDD using body mass index (BMI) as a control. The risk genes being tested were defined as genes showing genetic association, differential expression, or co-expression in psychiatric patient postmortem brains [76-94] (Fig. 5f, Supplementary Tables 6-8). We observed significant enrichment in DEGs of all three neuronal cell types (excitatory, GABA1, and GABA2 inhibitory neuron clusters) with ASD, SCZ, and BP-related gene sets. However, MDD and BMI did not show significant enrichment in the analysis. In excitatory neurons we found that 13 genes are shared in signals of genetics, DEGs, and COE level (*VAMP2, DDX1, KIF1A, KLC1, PPP6R2, ATP6V0A1, SV2A, AAK1, KIF1B, SLC8A1, SEZ6L2, ANK3, DDX24*). In GABA1

neurons, 5 genes are shared in signals of genetics, DEGs, and co-expression genes (COE) level (*DDX1, PPP6R2, LTBP1, AAK1, SEZ6L2*). In GABA2 neurons 10 genes are shared (*CARHSP1, TTC3, NREP, CPE, FABP5, CKB, PPP2R1A, AP2S1, S100A10, CADM1*) (Supplementary Fig. 12). These results suggest that convergent gene networks that are modified by the *NLGN3* R451C mutation play pivotal roles in the pathophysiology of mental disorders including SCZ, BP, and ASD.

DISCUSSION

Here we show that the R451C mutation of *NLGN3*, the first mutation identified in an ASD patient [8], increases excitatory, but not inhibitory, synaptic connectivity in human neurons. This phenotype was observed in human neurons both when analyzed in culture and when examined after transplantation into the mouse brain. Analyses of other neuronal parameters, such as neuronal dendrites or intrinsic electrical properties, uncovered no changes. We found that despite the fact that the R451C mutation decreases the levels of *NLGN3* protein, the increase in excitatory synaptic connectivity induced by this mutation is not associated with an ER stress response but represents a gain-of-function phenotype. Moreover, we describe that *NLGN3* R451C-mutant neurons exhibit major gene expression changes when compared to neurons derived from their parental ES cell line. Our findings thus show that in human neurons, the *NLGN3* R451C mutation causes a selective increase in excitatory synaptic function, suggesting a potential pathophysiological mechanism by which the R451C mutation induces ASDs. This hypothesis is strengthened by the finding that *NLGN3* knockout neurons showed a reduction in excitatory synaptic strength and overexpression of NLGN3 R451C recapitulated the synaptic enhancement in the excitatory synapses in human neuronal models.

NLGN3 is an adhesion molecule that is essential in mice for the normal function but not the formation of both excitatory and inhibitory synapses [65, 95-97]. Mutations in *NLGN* genes have been shown to induce ASDs and intellectual disability with an apparently 100% penetrance in multiple families [98-101]. In contrast, mutations in neurexins, especially *NRXN1*, predispose to a larger spectrum of neurodevelopmental disorders with a lower penetrance [28, 29, 102-104]. Although the *NLGN3* R451C mutation was intensely studied in knockin mice, little is known about its effect in human neurons. In the mice, the *Nlgn3* R451C-knockin mutation recapitulated, at least in part, the cognitive and motor behavior alterations seen in ASD subjects [12, 15, 16, 105, 106]. A series of detailed analyses in mice revealed that the R451C mutation induces region-, cell type-, and synapse-specific changes at both excitatory and inhibitory synapses that are consistent with gain-of-function and loss-of-function mechanisms at different synapses [12-14, 19]. For example, the *Nlgn3* R451C mutation enhanced inhibitory synaptic transmission in the cortex [12], but suppressed parvalbumin-positive inhibitory synapses in the hippocampus [19]. Furthermore, excitatory synaptic transmission was enhanced in hippocampal neurons and in cerebellar Purkinje cells [13, 14]. These data supported the hypothesis that *NLGN3* acts to specifying synapse properties in a manner that depends on the synaptic contact, suggesting that presynaptic *NLGN3*-binding partners are differentially expressed in different synapses may be crucial determinants of its role [7].

Extensive studies on the effect of the *Nlgn3* R451C mutation on synapses in mice have strongly supported a causative role for the R451C mutation in ASD pathophysiology, but it was unclear from these studies whether the results in mice actually translate to human neurons. Studies of human neurons carrying ASD-linked mutations in *NRXN1* [28, 29] or *NLGN4X* [30, 31] uncovered robust human-specific synaptic phenotypes, suggesting that the *NRXN-NLGN* adhesion complex may perform different roles in mice and humans. For example, heterozygous *NRXN1* deletions produced profound synaptic deficits in human neurons but not in mouse neurons that were generated by identical procedures [28, 29]. The goal of the current study, therefore, was to examine whether the *NLGN3* R451C mutation alters the function of synapses in human neurons similar to mouse neurons and whether there exists a novel mechanism specific to human neurons.

We found that in a human neuronal model system, i.e. excitatory and inhibitory iNs mixed cultures, the *NLGN3* R451C mutation augmented the strength of neurotransmission and increased the overall number of excitatory synapses (a gain-of-function phenotype), but had no major effect on inhibitory synapses (Figs. 1 and 2). Consistent with previous studies in mouse models [12], we also detected a lower expression level of NLGN3 in the R451C-mutant human neuronal cultures. To rule out the possibility of the “gain-of-function” in excitatory synaptic transmission in the R451C-mutant human neurons being a direct result of the loss of NLGN3 expression, we conducted synaptic physiology in *NLGN3* knockout human neurons. We found that NLGN3 ablation actually caused a decrease in excitatory synaptic release in neurons derived from two clones of *NLGN3* knockout pluripotent stem cells (Fig. 2j-m), but without a strong impact on synapse formation (Supplementary Fig. 4d). Moreover, overexpression of NLGN3 R451C in two pluripotent stem cell lines (both ES cells and iPS cells) recapitulated the enhanced excitatory synaptic transmission (Fig. 2n-s). Importantly, the hyper-glutamatergic transmission phenotype was maintained in *NLGN3* R451C-mutant neurons after they had been grafted into mouse brain (Fig. 4). Given the cell type- and region-specific effects of the mouse *Nlgn3* R451C mutation as discussed above, it is important to note that other types of human neurons might need to be considered to fully assess the impact of the *NLGN3* R451C mutation on the human brain. Although the detailed molecular mechanism by which the R451C mutation increases synaptic strength remains unknown, we hypothesize based on the observed phenotype that postsynaptic NLGN3 R451C neurons enhance presynaptic function via a retrograde signaling mechanism involving presynaptic neurexins. Neurexins were previously shown to engage in trans-synaptic signaling mechanisms [107, 108], suggesting a bidirectional organization of synapses based on neurexins as a central signaling molecule. Nevertheless, the current experiments establish that the observation of a gain-of-function effect of the *Nlgn3* R451C mutation in mouse neurons is transferable to human neurons, and that the *NLGN3* R451C mutation produces a profound and selective change in excitatory synaptic release in human neurons that could reasonably account for ASD pathogenesis.

Using single-cell gene expression profiling, we found that the *NLGN3* R451C mutation is associated with differential gene expression changes in excitatory and inhibitory human neurons. Excitatory *NLGN3* R451C-mutant neurons showed a higher synaptic function enrichment than inhibitory *NLGN3* R451C-mutant neurons. Furthermore, we found an upregulation of the presynaptic *NLGN3* binding partner *NRXN1*, which may enhance

synaptic function specifically in excitatory neurons. We conducted a comprehensive comparison between R451C DEGs and psychiatric disorders-related risk genes, taking advantage of numerous types of existing data, including genetic findings, differential expression, and co-expression studies (Supplementary Table 8) [76-94] to capture the different aspects of genetic, environmental, or gene–environmental interaction effects. Analysis of the gene networks represented by the specific DEGs of R451C-mutant neurons suggested that they associate strongly with ASD, SCZ, and BP but not with MDD and obesity. These data imply that different mental disorders may have convergent gene networks that affect neuronal functions including synaptic transmission in the brain [109]. We hypothesize that autism may be associated with dysregulated convergent gene networks, and ASD-related gene mutations in a single gene, such as *NLGN3*, may affect this convergent gene network function.

As any study, our experiments have inherent limitations. In this study, we used iN human neuronal model, which transdifferentiates pluripotent stem cells by ectopic expression of pro-neuronal differentiation factors Ngn2 (for excitatory) [36] and Ascl1/Dlx2 (for inhibitory) [37]. Previous studies have extensively characterized these neurons, including morphological, functional, and genomic analyses [28, 29, 36, 37]. This model may not be able to capture the developmental transitions that occur during neurodifferentiation. However, our previous study indicated that neurons generated from traditional neurodifferentiation carrying the *NRXN1* mutation recapitulated the synaptic phenotype observed in iN models [29]. A recent study [69] using single-cell transcriptomic analysis, found a diverse molecular heterogeneity in the neuronal cell types and found that the induction factor NGN2 expression level and the duration of NGN2 expression would bias the neuronal identity. It has been shown that combining NGN2 reprogramming with SMAD and WNT inhibition can generate patterned-induced neurons with some heterogeneity [68]. Our analysis also revealed the molecular heterogeneity of the neuronal cell types including molecularly undefined transition clusters, which is probably specific to the protocol we used. In this study, we analyzed the gene expression changes in the most mature clusters of excitatory and inhibitory neurons in the co-culture system, which we considered to be a more reliable approach compared to analyzing gene expression signatures in transition-stage neurons.

In this study we only considered a limited number of excitatory and inhibitory neuronal types, and also did not examine any glial cell types. *NLGN3* is also expressed in glial cells (Supplementary Fig. S1e) [61, 62]. The effect of the *NLGN3* R451C mutation on glial cell types and different brain region-specific human neurons requires further investigations. Furthermore, we have not explored the trafficking and expression of NLGN3 R451C-mutant protein in the human neurons, although extensive studies on this question were performed previously using heterologous expression approaches [10]. Nevertheless, we have explored the hypothesis that ER stress and UPR may be involved in the pathogenesis associated with R451C [14] but found no evidence for this hypothesis (Fig. 3).

Finally, it has been shown that derivation of genetically altered cell clones from human stem cells causes a profound change in gene expression because stem cells are undergoing continuous genetic changes in culture that are often subtle but accumulate during clonal

expansion [28]. As a result, the RNAseq profiles of neurons derived from a stem cell line and from wild-type clonal derivatives of that stem cell line differ dramatically [28]. Thus, the assessment of DEGs between neurons generated from parental stem cell lines and clonal mutant derivatives needs to be treated with caution, as these neurons are not truly isogenic and isogenicity can only be achieved with conditional manipulations. However, the fact that the DEGs we observed in our study between R451C-mutant and control neurons are consistent with a change in synaptic pathways is encouraging biological interpretation, although such an interpretation will remain subject to reservations until isogenic neurons are examined. It should be noted that this is a general problem in studies of gene expression changes of mutant neurons, and that a precise set of comparisons is often difficult to achieve.

In summary, the present study dissected the functional impact of the autism-related *NLGN3* R451C mutation on synaptic transmission in a human neuronal model system. The dramatic enhancement of excitatory synaptic connectivity by the *NLGN3* R451C mutation suggests a pathophysiological pathway in the development of ASDs whereby increases in cortical glutamatergic synaptic transmission may alter the overall excitatory/inhibitory balance, consistent with earlier hypotheses that changes in this balance are a major driver of neuropsychiatric disorders.

Supplementary Material

Refer to Web version on PubMed Central for supplementary material.

ACKNOWLEDGEMENTS

We thank the members of the Pang Lab for their insightful comments on the manuscript. We also thank Xueying Wang from Central South University for collecting the psychiatric risk summary gene list.

FUNDING

This study was supported by grants from the Robert Wood Johnson Foundation to the Child Health Institute of New Jersey (RWJF grant #74260), the Governor's Council for Medical Research and Treatment of Autism (CAUT14APL028 to ZPP; CAUT16APL020 to DC), and the NIMH (MH092931 to TCS; MH122519 to CP; MH126420 to ZPP), and by a predoctoral fellowship from the NIMH (F30MH108321 to VRM).

DATA AVAILABILITY

Single-cell-RNAseq data were deposited and available on the NCBI Gene Expression Omnibus under accession number GSE180751.

REFERENCES

1. Colvert E, Tick B, McEwen F, Stewart C, Curran SR, Woodhouse E, et al. Heritability of autism spectrum disorder in a UK population-based twin sample. JAMA Psychiatry. 2015;72:415–23. [PubMed: 25738232]
2. Geschwind DH, Flint J. Genetics and genomics of psychiatric disease. Science. 2015;349:1489–94. [PubMed: 26404826]
3. Sandin S, Lichtenstein P, Kuja-Halkola R, Larsson H, Hultman CM, Reichenberg A. The familial risk of autism. JAMA. 2014;311:1770–7. [PubMed: 24794370]

4. Skuse DH, Mandy WP, Scourfield J. Measuring autistic traits: heritability, reliability and validity of the Social and Communication Disorders Checklist. Br J Psychiatry. 2005;187:568–72. [PubMed: 16319410]
5. Zoghbi HY, Bear MF. Synaptic dysfunction in neurodevelopmental disorders associated with autism and intellectual disabilities. Cold Spring Harb Perspect Biol. 2012;4:a009886. [PubMed: 22258914]
6. Sudhof TC. Neuroligins and neurexins link synaptic function to cognitive disease. Nature. 2008;455:903–11. [PubMed: 18923512]
7. Sudhof TC. Synaptic neurexin complexes: a molecular code for the logic of neural circuits. Cell. 2017;171:745–69. [PubMed: 29100073]
8. Jamain S, Quach H, Betancur C, Rastam M, Colineaux C, Gillberg IC, et al. Mutations of the X-linked genes encoding neuroligins NLGN3 and NLGN4 are associated with autism. Nat Genet. 2003;34:27–9. [PubMed: 12669065]
9. Comoletti D, De Jaco A, Jennings LL, Flynn RE, Gaietta G, Tsigelny I, et al. The Arg451Cys-neuroligin-3 mutation associated with autism reveals a defect in protein processing. J Neurosci. 2004;24:4889–93. [PubMed: 15152050]
10. Chubykin AA, Liu X, Comoletti D, Tsigelny I, Taylor P, Sudhof TC. Dissection of synapse induction by neuroligins: effect of a neuroligin mutation associated with autism. J Biol Chem. 2005;280:22365–74. [PubMed: 15797875]
11. De Jaco A, Comoletti D, Kovarik Z, Gaietta G, Radic Z, Lockridge O, et al. A mutation linked with autism reveals a common mechanism of endoplasmic reticulum retention for the alpha,beta-hydrolase fold protein family. J Biol Chem. 2006;281:9667–76. [PubMed: 16434405]
12. Tabuchi K, Blundell J, Etherton MR, Hammer RE, Liu X, Powell CM, et al. A neuroligin-3 mutation implicated in autism increases inhibitory synaptic transmission in mice. Science. 2007;318:71–6. [PubMed: 17823315]
13. Etherton M, Foldy C, Sharma M, Tabuchi K, Liu X, Shamloo M, et al. Autism-linked neuroligin-3 R451C mutation differentially alters hippocampal and cortical synaptic function. Proc Natl Acad Sci USA. 2011;108:13764–9. [PubMed: 21808020]
14. Trobiani L, Favaloro FL, Di Castro MA, Di Mattia M, Cariello M, Miranda E, et al. UPR activation specifically modulates glutamate neurotransmission in the cerebellum of a mouse model of autism. Neurobiol Dis. 2018;120:139–50. [PubMed: 30201312]
15. Cao W, Lin S, Xia QQ, Du YL, Yang Q, Zhang MY, et al. Gamma oscillation dysfunction in mPFC leads to social deficits in neuroligin 3 R451C knockin mice. Neuron. 2018;97:1253–60.e1257. [PubMed: 29503190]
16. Rothwell PE, Fuccillo MV, Maxeiner S, Hayton SJ, Gokce O, Lim BK, et al. Autism-associated neuroligin-3 mutations commonly impair striatal circuits to boost repetitive behaviors. Cell. 2014;158:198–212. [PubMed: 24995986]
17. Chadman KK, Gong S, Scattoni ML, Boltuck SE, Gandhy SU, Heintz N, et al. Minimal aberrant behavioral phenotypes of neuroligin-3 R451C knockin mice. Autism Res. 2008;1:147–58. [PubMed: 19360662]
18. De Jaco A, Dubi N, Comoletti D, Taylor P. Folding anomalies of neuroligin3 caused by a mutation in the alpha/beta-hydrolase fold domain. Chem Biol Interact. 2010;187:56–8. [PubMed: 20227402]
19. Foldy C, Malenka RC, Sudhof TC. Autism-associated neuroligin-3 mutations commonly disrupt tonic endocannabinoid signaling. Neuron. 2013;78:498–509. [PubMed: 23583622]
20. Okita K, Ichisaka T, Yamanaka S. Generation of germline-competent induced pluripotent stem cells. Nature. 2007;448:313–7. [PubMed: 17554338]
21. Takahashi K, Tanabe K, Ohnuki M, Narita M, Ichisaka T, Tomoda K, et al. Induction of pluripotent stem cells from adult human fibroblasts by defined factors. Cell. 2007;131:861–72. [PubMed: 18035408]
22. Takahashi K, Yamanaka S. Induction of pluripotent stem cells from mouse embryonic and adult fibroblast cultures by defined factors. Cell. 2006;126:663–76. [PubMed: 16904174]
23. Wernig M, Meissner A, Foreman R, Brambrink T, Ku M, Hochedlinger K, et al. In vitro reprogramming of fibroblasts into a pluripotent ES-cell-like state. Nature. 2007;448:318–24. [PubMed: 17554336]

24. Yi F, Danko T, Botelho SC, Patzke C, Pak C, Wernig M, et al. Autism-associated SHANK3 haploinsufficiency causes Ih channelopathy in human neurons. Science. 2016;352:aaf2669. [PubMed: 26966193]
25. Shcheglovitov A, Shcheglovitova O, Yazawa M, Portmann T, Shu R, Sebastiano V, et al. SHANK3 and IGF1 restore synaptic deficits in neurons from 22q13 deletion syndrome patients. Nature. 2013;503:267–71. [PubMed: 24132240]
26. Chiola S, Napan KL, Wang Y, Lazarenko RM, Armstrong CJ, Cui J, et al. Defective AMPA-mediated synaptic transmission and morphology in human neurons with hemizygous SHANK3 deletion engrafted in mouse prefrontal cortex. Mol Psychiatry. 2021.
27. Soliman MA, Aboharb F, Zeltner N, Studer L. Pluripotent stem cells in neuropsychiatric disorders. Mol Psychiatry. 2017;22:1241–9. [PubMed: 28322279]
28. Pak C, Danko T, Mirabella VR, Wang J, Liu Y, Vangipuram M, et al. Cross-platform validation of neurotransmitter release impairments in schizophrenia patient-derived NRXN1-mutant neurons. Proc Natl Acad Sci USA. 2021;118:e2025598118. [PubMed: 34035170]
29. Pak C, Danko T, Zhang Y, Aoto J, Anderson G, Maxeiner S, et al. Human neuropsychiatric disease modeling using conditional deletion reveals synaptic transmission defects caused by heterozygous mutations in NRXN1. Cell Stem Cell. 2015;17:316–28. [PubMed: 26279266]
30. Marro SG, Chanda S, Yang N, Janas JA, Valperga G, Trotter J, et al. Neuroligin-4 regulates excitatory synaptic transmission in human. Neurons Neuron. 2019;103:617–26.e616. [PubMed: 31257103]
31. Cast TP, Boesch DJ, Smyth K, Shaw AE, Ghebrial M, Chanda S. An autism-associated mutation impairs neuroligin-4 glycosylation and enhances excitatory synaptic transmission in human neurons. J Neurosci. 2021;41:392–407. [PubMed: 33268543]
32. Halikere A, Popova D, Scarnati MS, Hamod A, Swerdel MR, Moore JC, et al. Addiction associated N40D mu-opioid receptor variant modulates synaptic function in human neurons. Mol Psychiatry. 2020;25:1406–19. [PubMed: 31481756]
33. Ran FA, Hsu PD, Wright J, Agarwala V, Scott DA, Zhang F. Genome engineering using the CRISPR-Cas9 system. Nat Protoc. 2013;8:2281–308. [PubMed: 24157548]
34. Marro S, Yang N. Transdifferentiation of mouse fibroblasts and hepatocytes to functional neurons. Methods Mol Biol. 2014;1150:237–46. [PubMed: 24744003]
35. Pang ZP, Yang N, Vierbuchen T, Ostermeier A, Fuentes DR, Yang TQ, et al. Induction of human neuronal cells by defined transcription factors. Nature. 2011;476:220–3. [PubMed: 21617644]
36. Zhang Y, Pak C, Han Y, Ahlenius H, Zhang Z, Chanda S, et al. Rapid single-step induction of functional neurons from human pluripotent stem cells. Neuron. 2013;78:785–98. [PubMed: 23764284]
37. Yang N, Chanda S, Marro S, Ng YH, Janas JA, Haag D, et al. Generation of pure GABAergic neurons by transcription factor programming. Nat Methods. 2017;14:621–8. [PubMed: 28504679]
38. Xu R, Brawner AT, Li S, Liu JJ, Kim H, Xue H, et al. OLIG2 drives abnormal neurodevelopmental phenotypes in human iPSC-based organoid and chimeric mouse models of down syndrome. Cell Stem Cell. 2019;24:908–26.e908. [PubMed: 31130512]
39. Xu R, Li X, Boreland AJ, Posyton A, Kwan K, Hart RP, et al. Human iPSC-derived mature microglia retain their identity and functionally integrate in the chimeric mouse brain. Nat Commun. 2020;11:1577. [PubMed: 32221280]
40. Fantuzzo JA, Mirabella VR, Hamod AH, Hart RP, Zahn JD, Pang ZP. Intellicount: high-throughput quantification of fluorescent synaptic protein puncta by machine learning. eNeuro. 2017;4:ENEURO.0219–17.2017.
41. Schneider CA, Rasband WS, Eliceiri KW. NIH Image to ImageJ: 25 years of image analysis. Nat Methods. 2012;9:671–5. [PubMed: 22930834]
42. Yalcin B, Zhao L, Stofanko M, O'Sullivan NC, Kang ZH, Roost A, et al. Modeling of axonal endoplasmic reticulum network by spastic paraplegia proteins. Elife. 2017;6:e23882. [PubMed: 28742022]
43. Pang ZP, Xu W, Cao P, Sudhof TC. Calmodulin suppresses synaptotagmin-2 transcription in cortical neurons. J Biol Chem. 2010;285:33930–9. [PubMed: 20729199]

44. Uchigashima M, Leung M, Watanabe T, Cheung A, Le T, Pallat S, et al. Neuroligin3 splice isoforms shape inhibitory synaptic function in the mouse hippocampus. J Biol Chem. 2020;295:8589–95. [PubMed: 32381505]
45. Liu J, Conde K, Zhang P, Lilascharoen V, Xu Z, Lim BK, et al. Enhanced AMPA receptor trafficking mediates the anorexigenic effect of endogenous glucagon-like peptide-1 in the paraventricular hypothalamus. Neuron. 2017;96:897–909.e895. [PubMed: 29056294]
46. Maximov A, Pang ZP, Tervo DG, Sudhof TC. Monitoring synaptic transmission in primary neuronal cultures using local extracellular stimulation. J Neurosci Methods. 2007;161:75–87. [PubMed: 17118459]
47. Bahl E, Koomar T, Michaelson JJ. cerebroViz: an R package for anatomical visualization of spatiotemporal brain data. Bioinformatics. 2017;33:762–3. [PubMed: 28011779]
48. Butler A, Hoffman P, Smibert P, Papalexi E, Satija R. Integrating single-cell transcriptomic data across different conditions, technologies, and species. Nat Biotechnol. 2018;36:411–20. [PubMed: 29608179]
49. Satija R, Farrell JA, Gennert D, Schier AF, Regev A. Spatial reconstruction of single-cell gene expression data. Nat Biotechnol. 2015;33:495–502. [PubMed: 25867923]
50. Nowakowski TJ, Bhaduri A, Pollen AA, Alvarado B, Mostajo-Radji MA, Di Lullo E, et al. Spatiotemporal gene expression trajectories reveal developmental hierarchies of the human cortex. Science. 2017;358:1318–23. [PubMed: 29217575]
51. Ianevski A, Giri AK, Aittokallio T. Fully-automated and ultra-fast cell-type identification using specific marker combinations from single-cell transcriptomic data. Nat Commun. 2022;13:1246. [PubMed: 35273156]
52. Polioudakis D, de la Torre-Ubieta L, Langerman J, Elkins AG, Shi X, Stein JL, et al. A single-cell transcriptomic atlas of human neocortical development during mid-gestation. Neuron. 2019;103:785–801.e788. [PubMed: 31303374]
53. Weissbein U, Schachter M, Egli D, Benvenisty N. Analysis of chromosomal aberrations and recombination by allelic bias in RNA-Seq. Nat Commun. 2016;7:12144. [PubMed: 27385103]
54. DePristo MA, Banks E, Poplin R, Garimella KV, Maguire JR, Hartl C, et al. A framework for variation discovery and genotyping using next-generation DNA sequencing data. Nat Genet. 2011;43:491–8. [PubMed: 21478889]
55. Koopmans F, van Nierop P, Andres-Alonso M, Byrnes A, Cijsouw T, Coba MP, et al. SynGO: an evidence-based, expert-curated knowledge base for the synapse. Neuron. 2019;103:217–34.e214. [PubMed: 31171447]
56. Jin S, Guerrero-Juarez CF, Zhang L, Chang I, Ramos R, Kuan CH, et al. Inference and analysis of cell-cell communication using CellChat. Nat Commun. 2021;12:1088. [PubMed: 33597522]
57. Szklarczyk D, Gable AL, Lyon D, Junge A, Wyder S, Huerta-Cepas J, et al. STRING v11: protein-protein association networks with increased coverage, supporting functional discovery in genome-wide experimental datasets. Nucleic Acids Res. 2019;47:D607–D613. [PubMed: 30476243]
58. Consortium GT. The genotype-tissue expression (GTEx) project. Nat Genet. 2013;45:580–5. [PubMed: 23715323]
59. Miller JA, Ding SL, Sunkin SM, Smith KA, Ng L, Szafer A, et al. Transcriptional landscape of the prenatal human brain. Nature. 2014;508:199–206. [PubMed: 24695229]
60. Satterstrom FK, Kosmicki JA, Wang J, Breen MS, De Rubeis S, An JY, et al. Large- scale exome sequencing study implicates both developmental and functional changes in the neurobiology of autism. Cell. 2020;180:568–84.e523. [PubMed: 31981491]
61. Gilbert M, Smith J, Roskams AJ, Auld VJ. Neuroligin 3 is a vertebrate gliotactin expressed in the olfactory ensheathing glia, a growth-promoting class of macroglia. Glia. 2001;34:151–64. [PubMed: 11329178]
62. Zhang Y, Chen K, Sloan SA, Bennett ML, Scholze AR, O'Keeffe S, et al. An RNA-sequencing transcriptome and splicing database of glia, neurons, and vascular cells of the cerebral cortex. J Neurosci. 2014;34:11929–47. [PubMed: 25186741]
63. Velmeshev D, Schirmer L, Jung D, Haeussler M, Perez Y, Mayer S, et al. Single-cell genomics identifies cell type-specific molecular changes in autism. Science. 2019;364:685–9. [PubMed: 31097668]

64. Craig AM, Kang Y. Neurexin-neuroligin signaling in synapse development. Curr Opin Neurobiol. 2007;17:43–52. [PubMed: 17275284]

65. Varoqueaux F, Aramuni G, Rawson RL, Mohrmann R, Missler M, Gottmann K, et al. Neuroligins determine synapse maturation and function. Neuron. 2006;51:741–54. [PubMed: 16982420]

66. Wu H, Xu J, Pang ZP, Ge W, Kim KJ, Blanchi B, et al. Integrative genomic and functional analyses reveal neuronal subtype differentiation bias in human embryonic stem cell lines. Proc Natl Acad Sci USA. 2007;104:13821–6. [PubMed: 17693548]

67. Ulbrich L, Favaloro FL, Trobiani L, Marchetti V, Patel V, Pascucci T, et al. Autism-associated R451C mutation in neuroligin3 leads to activation of the unfolded protein response in a PC12 Tet-On inducible system. Biochem J. 2016;473:423–34. [PubMed: 26621873]

68. Nehme R, Zuccaro E, Ghosh SD, Li C, Sherwood JL, Pietilainen O, et al. Combining NGN2 programming with developmental patterning generates human excitatory neurons with NMDAR-mediated synaptic transmission. Cell Rep. 2018;23:2509–23. [PubMed: 29791859]

69. Lin HC, He Z, Ebert S, Schornig M, Santel M, Nikolova MT, et al. NGN2 induces diverse neuron types from human µluripotency. Stem Cell Rep. 2021;16:2118–27.

70. Zhang S, Zhang H, Zhou Y, Qiao M, Zhao S, Kozlova A, et al. Allele-specific open chromatin in human iPSC neurons elucidates functional disease variants. Science. 2020;369:561–5. [PubMed: 32732423]

71. Hata Y, Butz S, Sudhof TC. CASK: a novel dlg/PSD95 homolog with an N-terminal calmodulin-dependent protein kinase domain identified by interaction with neurexins. J Neurosci. 1996;16:2488–94. [PubMed: 8786425]

72. Najm J, Horn D, Wimplinger I, Golden JA, Chizhikov VV, Sudi J, et al. Mutations of CASK cause an X-linked brain malformation phenotype with microcephaly and hypoplasia of the brainstem and cerebellum. Nat Genet. 2008;40:1065–7. [PubMed: 19165920]

73. Hackett A, Tarpey PS, Licata A, Cox J, Whibley A, Boyle J, et al. CASK mutations are frequent in males and cause X-linked nystagmus and variable XLMR phenotypes. Eur J Hum Genet. 2010;18:544–52. [PubMed: 20029458]

74. Sanders SJ, Murtha MT, Gupta AR, Murdoch JD, Raubeson MJ, Willsey AJ, et al. De novo mutations revealed by whole-exome sequencing are strongly associated with autism. Nature. 2012;485:237–41. [PubMed: 22495306]

75. Atasoy D, Schoch S, Ho A, Nadasy KA, Liu X, Zhang W, et al. Deletion of CASK in mice is lethal and impairs synaptic function. Proc Natl Acad Sci USA. 2007;104:2525–30. [PubMed: 17287346]

76. Basu SN, Kollu R, Banerjee-Basu S. AutDB: a gene reference resource for autism research. Nucleic Acids Res. 2009;37:D832–6. [PubMed: 19015121]

77. Darnell JC, Van Driesche SJ, Zhang C, Hung KY, Mele A, Fraser CE, et al. FMRP stalls ribosomal translocation on mRNAs linked to synaptic function and autism. Cell. 2011;146:247–61. [PubMed: 21784246]

78. Li J, Cai T, Jiang Y, Chen H, He X, Chen C, et al. Genes with de novo mutations are shared by four neuropsychiatric disorders discovered from NPdenovo database. Mol Psychiatry. 2016;21:290–7. [PubMed: 25849321]

79. Gandal MJ, Haney JR, Parikshak NN, Leppa V, Ramaswami G, Hartl C, et al. Shared molecular neuropathology across major psychiatric disorders parallels polygenic overlap. Science. 2018;359:693–7. [PubMed: 29439242]

80. Voineagu I, Wang X, Johnston P, Lowe JK, Tian Y, Horvath S, et al. Transcriptomic analysis of autistic brain reveals convergent molecular pathology. Nature. 2011;474:380–4. [PubMed: 21614001]

81. Gupta S, Ellis SE, Ashar FN, Moes A, Bader JS, Zhan J, et al. Transcriptome analysis reveals dysregulation of innate immune response genes and neuronal activity-dependent genes in autism. Nat Commun. 2014;5:5748. [PubMed: 25494366]

82. Marshall CR, Howrigan DP, Merico D, Thiruvahindrapuram B, Wu W, Greer DS, et al. Contribution of copy number variants to schizophrenia from a genome-wide study of 41,321 subjects. Nat Genet. 2017;49:27–35. [PubMed: 27869829]

83. Ayalew M, Le-Niculescu H, Levey DF, Jain N, Changala B, Patel SD, et al. Convergent functional genomics of schizophrenia: from comprehensive understanding to genetic risk prediction. Mol Psychiatry. 2012;17:887–905. [PubMed: 22584867]
84. Luo XJ, Mattheisen M, Li M, Huang L, Rietschel M, Borglum AD, et al. Systematic integration of brain eQTL and GWAS Identifies ZNF323 as a novel schizophrenia risk gene and suggests recent positive selection based on compensatory advantage on pulmonary function. Schizophr Bull. 2015;41:1294–308. [PubMed: 25759474]
85. Parikshak NN, Swarup V, Belgard TG, Irimia M, Ramaswami G, Gandal MJ, et al. Genome-wide changes in lncRNA, splicing, and regional gene expression patterns in autism. Nature. 2016;540:423–7. [PubMed: 27919067]
86. Gandal MJ, Zhang P, Hadjimichael E, Walker RL, Chen C, Liu S, et al. Transcriptome-wide isoform-level dysregulation in ASD, schizophrenia, and bipolar disorder. Science. 2018;362:eaat8127. [PubMed: 30545856]
87. Charney AW, Stahl EA, Green EK, Chen CY, Moran JL, Chambert K, et al. Contribution of rare copy number variants to bipolar disorder risk is limited to schizoaffective cases. Biol Psychiatry. 2019;86:110–9. [PubMed: 30686506]
88. Locke AE, Kahali B, Berndt SI, Justice AE, Pers TH, Day FR, et al. Genetic studies of body mass index yield new insights for obesity biology. Nature. 2015;518:197–206. [PubMed: 25673413]
89. Lewis CM, Levinson DF, Wise LH, DeLisi LE, Straub RE, Hovatta I, et al. Genome scan meta-analysis of schizophrenia and bipolar disorder, part II: Schizophrenia. Am J Hum Genet. 2003;73:34–48. [PubMed: 12802786]
90. Ng MY, Levinson DF, Faraone SV, Suarez BK, DeLisi LE, Arinami T, et al. Meta-analysis of 32 genome-wide linkage studies of schizophrenia. Mol Psychiatry. 2009;14:774–85. [PubMed: 19349958]
91. Allen NC, Bagade S, McQueen MB, Ioannidis JP, Kavvoura FK, Khoury MJ, et al. Systematic meta-analyses and field synopsis of genetic association studies in schizophrenia: the SzGene database. Nat Genet. 2008;40:827–34. [PubMed: 18583979]
92. Sun J, Kuo PH, Riley BP, Kendler KS, Zhao Z. Candidate genes for schizophrenia: a survey of association studies and gene ranking. Am J Med Genet B Neuropsychiatr Genet. 2008;147B:1173–81. [PubMed: 18361404]
93. Schizophrenia Working Group of the Psychiatric Genomics C. Biological insights from 108 schizophrenia-associated genetic loci. Nature. 2014;511:421–7. [PubMed: 25056061]
94. Lamparter D, Marbach D, Rueedi R, Kutalik Z, Bergmann S. Fast and rigorous computation of gene and pathway scores from SNP-based summary statistics. PLoS Comput Biol. 2016;12:e1004714. [PubMed: 26808494]
95. Chanda S, Hale WD, Zhang B, Wernig M, Sudhof TC. Unique versus redundant functions of neuroligin genes in shaping excitatory and inhibitory synapse properties. J Neurosci. 2017;37:6816–36. [PubMed: 28607166]
96. Zhang B, Sudhof TC. Neuroligins are selectively essential for NMDAR signaling in cerebellar stellate interneurons. J Neurosci. 2016;36:9070–83. [PubMed: 27581450]
97. Chih B, Engelman H, Scheiffele P. Control of excitatory and inhibitory synapse formation by neuroligins. Science. 2005;307:1324–8. [PubMed: 15681343]
98. Zhang C, Milunsky JM, Newton S, Ko J, Zhao G, Maher TA, et al. A neuroligin-4 missense mutation associated with autism impairs neuroligin-4 folding and endoplasmic reticulum export. J Neurosci. 2009;29:10843–54. [PubMed: 19726642]
99. Chanda S, Marro S, Wernig M, Sudhof TC. Neurons generated by direct conversion of fibroblasts reproduce synaptic phenotype caused by autism-associated neuroligin-3 mutation. Proc Natl Acad Sci USA. 2013;110:16622–7. [PubMed: 24046374]
100. Zhang B, Seigneur E, Wei P, Gokce O, Morgan J, Sudhof TC. Developmental plasticity shapes synaptic phenotypes of autism-associated neuroligin-3 mutations in the calyx of Held. Mol Psychiatry. 2017;22:1483–91. [PubMed: 27725662]
101. Laumonnier F, Bonnet-Brilhault F, Gomot M, Blanc R, David A, Moizard MP, et al. X-linked mental retardation and autism are associated with a mutation in the NLGN4 gene, a member of the neuroligin family. Am J Hum Genet. 2004;74:552–7. [PubMed: 14963808]

102. Geschwind DH, State MW. Gene hunting in autism spectrum disorder: on the path to precision medicine. Lancet Neurol. 2015;14:1109–20. [PubMed: 25891009]

103. Hu Z, Xiao X, Zhang Z, Li M. Genetic insights and neurobiological implications from NRXN1 in neuropsychiatric disorders. Mol Psychiatry. 2019;24:1400–14. [PubMed: 31138894]

104. Alliey-Rodriguez N, Grey TA, Shafee R, Asif H, Lutz O, Bolo NR, et al. NRXN1 is associated with enlargement of the temporal horns of the lateral ventricles in psychosis. Transl Psychiatry. 2019;9:230. [PubMed: 31530798]

105. Jaramillo TC, Liu S, Pettersen A, Birnbaum SG, Powell CM. Autism-related neuroligin-3 mutation alters social behavior and spatial learning. Autism Res. 2014;7:264–72. [PubMed: 24619977]

106. Norris RHC, Churilov L, Hannan AJ, Nithianantharajah J. Mutations in neuroligin-3 in male mice impact behavioral flexibility but not relational memory in a touchscreen test of visual transitive inference. Mol Autism. 2019;10:42. [PubMed: 31827744]

107. Aoto J, Martinelli DC, Malenka RC, Tabuchi K, Sudhof TC. Presynaptic neurexin-3 alternative splicing trans-synaptically controls postsynaptic AMPA receptor trafficking. Cell. 2013;154:75–88. [PubMed: 23827676]

108. Wittenmayer N, Korber C, Liu H, Kremer T, Varoqueaux F, Chapman ER, et al. Postsynaptic Neuroligin1 regulates presynaptic maturation. Proc Natl Acad Sci USA. 2009;106:13564–9. [PubMed: 19628693]

109. Brainstorm C, Anttila V, Bulik-Sullivan B, Finucane HK, Walters RK, Bras J, et al. Analysis of shared heritability in common disorders of the brain. Science 2018;360:eaap8757. [PubMed: 29930110]

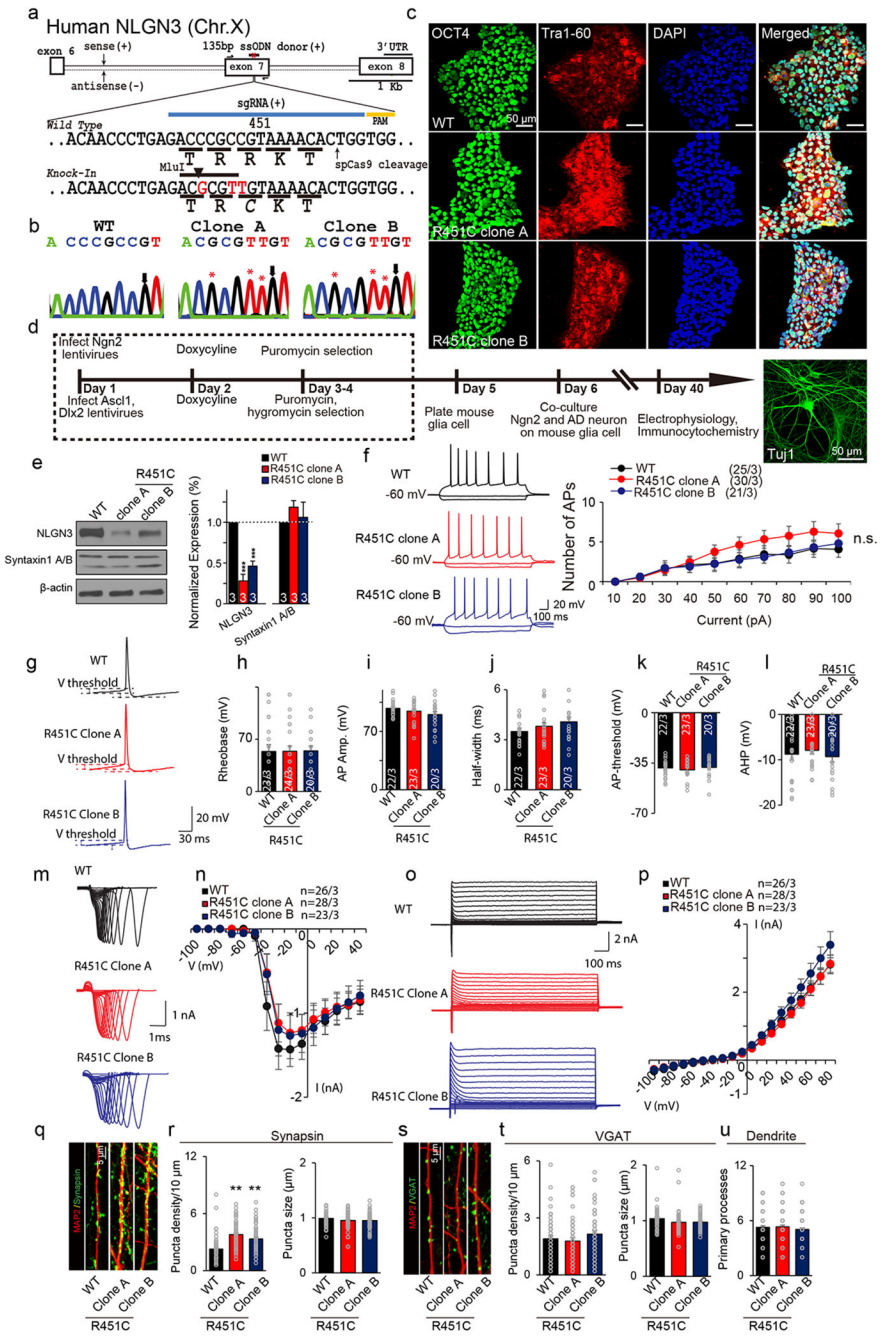

Fig. 1. NLGN3 R451C mixed culture of induced neuronal (iN) cells.

a NLGN3 R451C targeting strategy. The blue line indicates the sgRNA sequences, and the yellow line is the PAM. 135 bp single-stranded oligodeoxynucleotide (ssODNs) is the base for direct homologous recombination of NLGN3 exon 7 genomic sequence. We inserted a Mlu1 restriction site for genotyping. **b** Confirmation of NLGN3 R451C knockin cell lines by Sanger sequencing. * indicates mutated nucleotide. **c** Immunostaining of stem cell marker genes in control and converted ES cell lines. DAPI was used to visualize the cell nucleus. OCT4 (green) is expressed in the nucleus colocalized with DAPI, and Tra-160 (red) is expressed in the cell body. **d** Experimental design of *Ngn2* (GFP) and *Ascl1,*

Dlx2 (mCherry) iNs mixed culture paradigm. **e** Quantification of NLGN3 and Syntaxin protein expression levels in mixed culture of iN cells, $N = 3$. **f** Representative traces and quantification plot of step current injection action potential firing number. **g** Representative traces of Action Potentials (AP) recorded from control and R451C-iNs. Summary graphs of Rheobase (**h**), AP amplitude (**i**), AP half-width (**j**), AP threshold (**k**), and hyperpolarization potential (AHP) amplitude (**l**). Representative traces (**m**) and quantification (**n**) of whole-cell voltage-dependent sodium currents in control and R451C-iNs. Representative traces (**o**) and quantification (**p**) of whole-cell voltage-dependent potassium currents in control and R451C-iNs. **q** Representative images of synaptic puncta (labeled by synapsin immunofluorescence, green) associated with dendrites (visualized by MAP2 immunofluorescence, red) in control and R451C-iNs. **r** Quantification of synapsin puncta densities per 10 μm ($n = 60$) and puncta sizes (Synapsin, $n = 60$). **s** Representative images of inhibitory synapses immunolabeled with VGAT (green) and MAP2 (red) in control and R451C-iNs. **t** Quantification of VGAT puncta densities per 10 μm ($n = 60$), puncta sizes (VGAT, $n = 60$). **u** Quantification of primary dendrite numbers ($n = 60$) in control and R451C-iNs. Data are depicted as means ± SEM. Statistical significance was assessed by one-way ANOVA (**$P < 0.01$).

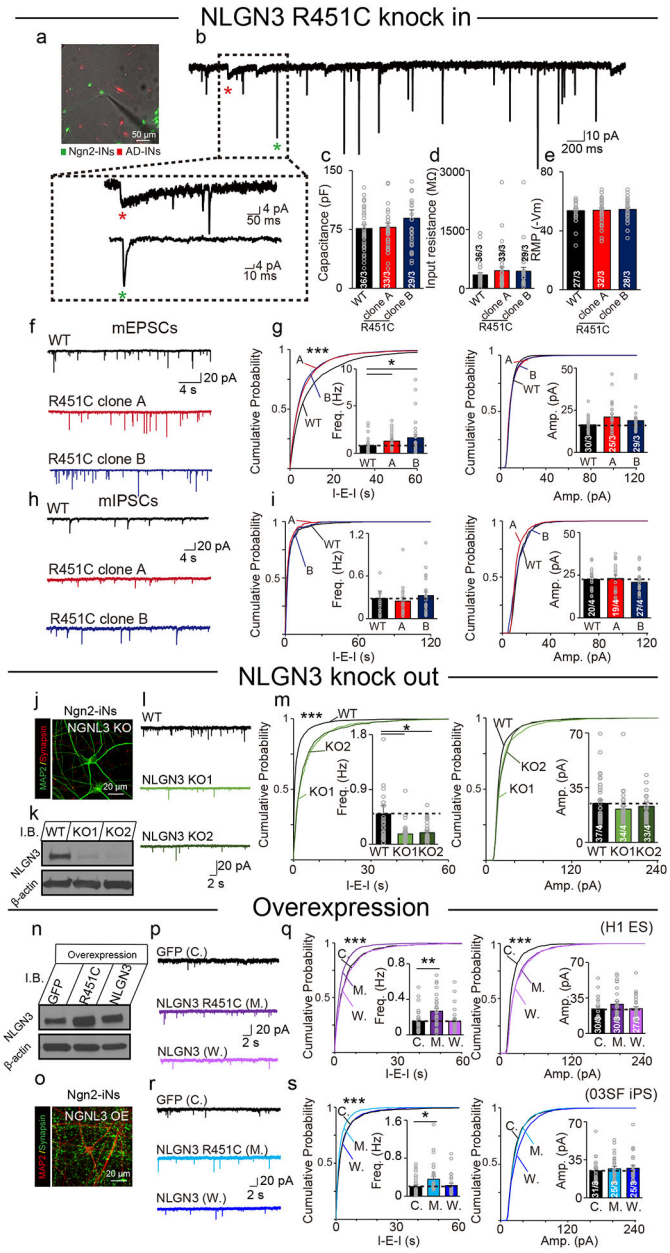

Fig. 2. NLGN3 R451C increases excitatory neurotransmission in vitro.

a Representative image of recording mixed culture iNs. Green cells are *Ngn2* iNs, red cells are *Ascl1* and *Dlx2* iNs. **b** Representative sPSC trace of mixed culture iNs. Green * indicate EPSC-like event, red * indicates IPSC-like event. **c**–**e** Intrinsic electrophysiology characterization of control and converted R451C-iNs. Summary of passive membrane properties (capacitance, input resistance, resting membrane potential). **f** Representative traces of mEPSCs (with 1 μM TTX and 50 μM PTX) in control and R451C human iNs**. g** Cumulative distribution and quantification (*inserts*) of mEPSC frequency (inter-event-interval, I-E-I, left panel) and amplitude (*right panel*) of mEPSCs in control and R451C-iNs. **h** Representative traces of mIPSCs (with 1 μM TTX and 20 μM CNQX) in control and R451C human iNs**. i** Cumulative distribution and quantification (*inserts*) of mIPSC

frequency (left panel) and amplitude (right panel). **j** Representative images of control and NLGN3 knockout (KO) iNs. **k** NLGN3 expression level in control and NLGN3 KO Ngn2-iNs. **l** Representative traces of mEPSCs in control and NLGN3 KO iNs. **m** Cumulative distribution and quantification (inserts) of mEPSCs frequency (left panel) amplitudes (right panel) in control and NLGN3 KO iNs. **n** Overexpression of human wild type- and R451C NLGN3 in Ngn2-iNs. **o** Representative neuronal images of Ngn2 iNs with overexpression of human NLGN3 R451C. **p** Representative traces of mEPSCs in control, NLGN3, and NLGN3 R451C overexpression-Ngn2 iNs generated from H1 ES cell line. **q** Cumulative distribution and quantification (inserts) of mEPSC frequency (left panel) and amplitude (right panel) in control (C.), NLGN3 R451C overexpression (M.), wild type NLGN3 overexpression (W.) iNs derived from H1 ES cell line. **r** Representative traces of mEPSCs in control, NLGN3, and NLGN3 R451C overexpression-Ngn2 iNs generated from iPS cell line. **q** Cumulative distribution and quantification (*inserts*) of mEPSC frequency (left panel) and amplitude (right panel) in control (C.), NLGN3 R451C overexpression (M.), wild type NLGN3 overexpression (W.) iNs derived from iPS cell line. Data are mean ± SEM; Number of cultured cells/ cultured batches are shown in bars. Statistical significance (*$p < 0.05$, **$p < 0.01$) was evaluated with the Kolmogorov–Smirnov test (cumulative probability plots) and one-way ANOVA (bar graphs).

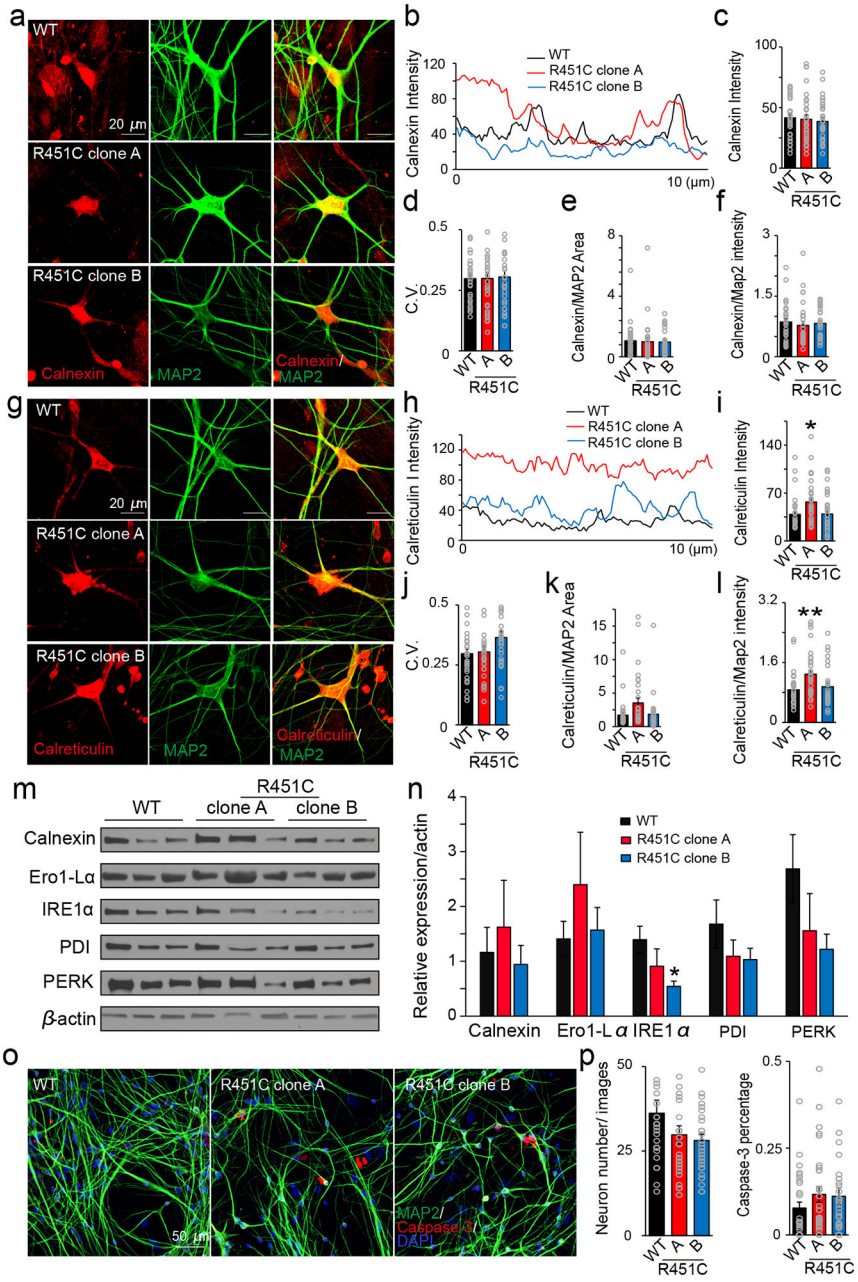

Fig. 3. No major ER stress found in human neurons carrying NLGN3 R451C mutation.

a Representative images of Calnexin (red) and MAP2 (red) in R451C and control iNs. **b–d** Calnexin intensity and distribution over 10 μm line for each cell. **e**, **f** Somatic Calnexin area and intensity normalized with MAP2 signals. **g** Representative images of Calreticulin (red) and MAP2 (red) in control and R451C-iNs. **h–j** Calreticulin intensity and distribution over 10 μm line for each cell. **k**, **l** Somatic Calreticulin area and intensity normalized with MAP2. **m** Analysis of ER stress markers (immunoblot) in the excitatory-inhibitory co-cultured iNs. **n** Quantification of ER stress markers protein expression level $N = 6$, 3 cultures 2 repeats. **o** Representative images of Caspase-3 (red), MAP2 (green), and DAPI human neurons carrying wild-type or R451C NLGN3. **p** Quantification of neuronal density

(DAPI and MAP) and Caspase-3^+ cells. Statistical significance (*$p < 0.05$; **$p < 0.01$) was evaluated with Student's *t*-test (bar graphs).

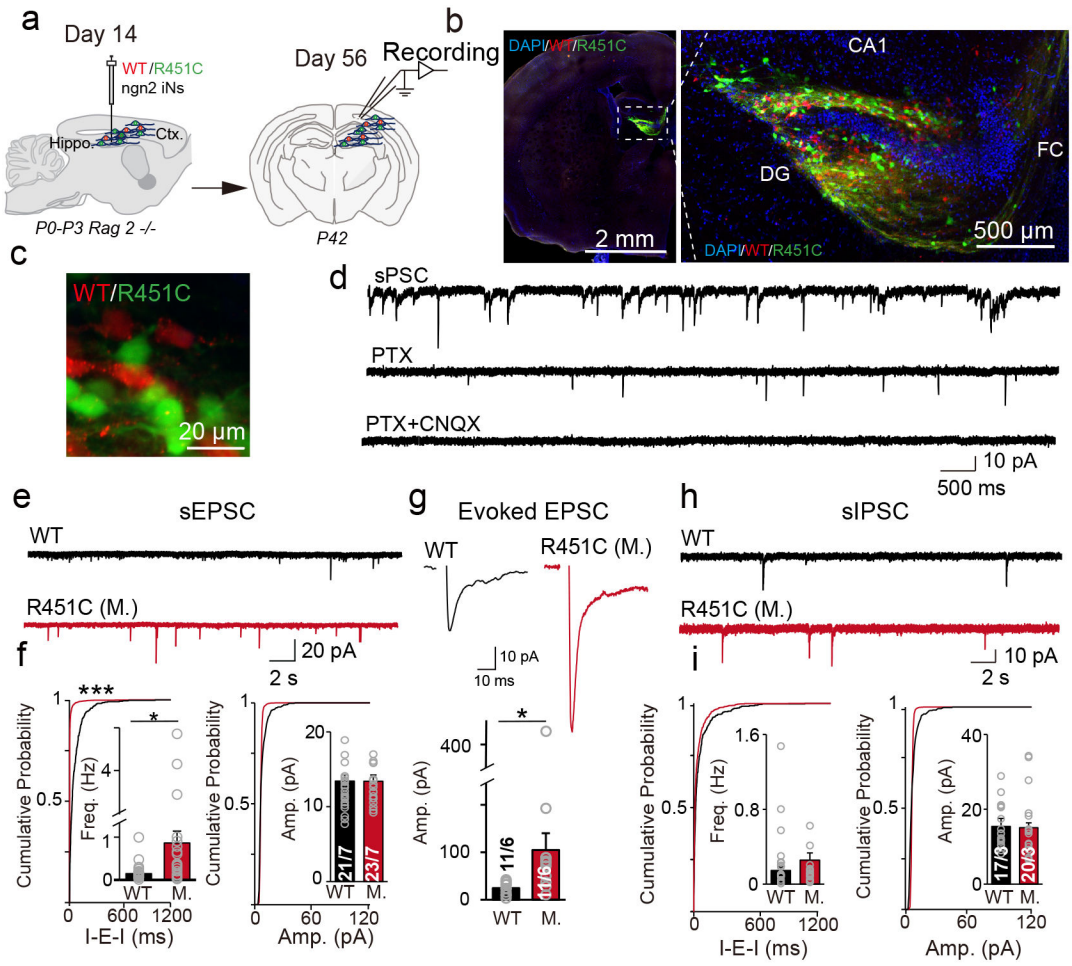

Fig. 4. Dual-color genotype transplantation of ESC H1 and NLGN3 R451C human iN cells in vivo.

a Experimental design of control (mCherry) and R451C (mVenus) iNs transplant in vivo. **b** Representative images of iN cells transplanted in Rag$^{2-/-}$ hippocampal region, a control line (mCherry), and R451C lines (mVenus). **c** Representative images of control and R451C converted iNs in vivo. **d** Representative sPSC trace of transplanted iNs in vivo. Slow responses could be blocked by picrotoxin (PTX). In the presence of PTX and CNQX (both 50 μM), no spontaneous activities were observed. **e** Representative sEPSC trace of control/R451C in vivo. **f** Quantification of sEPSC frequency and amplitude in vivo. **g** Representative trace and quantification of evoked EPSCs. **h** Representative sIPSC trace of control/R451C in vivo. **i** Quantification of sIPSC frequency and amplitude in vivo. The black and red bar represents control ES cell line and R451C converted cell lines. Data are mean + SEM; Numbers of cultured cells/ culture batches are shown in bars. Statistical significance (*$p <$ 0.05) was evaluated with the Kolmogorov–Smirnov test (cumulative probability plots) and one-way ANOVA (bar graphs).

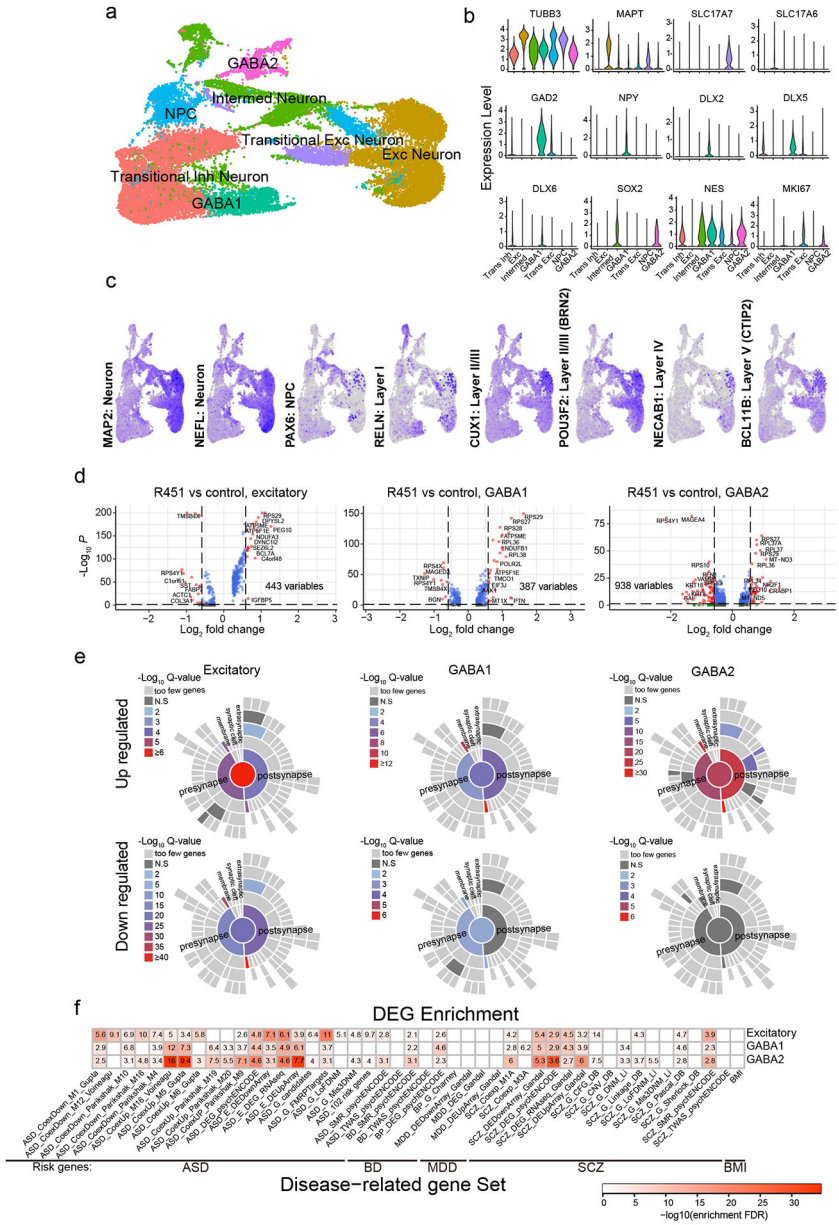

Fig. 5. Single-cell RNA seq of E/I mixed culture R451C human iNs.

a UMAP of all human neuronal cells (n = 27,724) reveals seven distinct neuronal subtypes. **b** Expression levels of human neuron and progenitor marker for each neuronal subtype. **c** Human induced neurons express mature neuron and cortical layer marker features. **d** DEGs in R451C versus control in excitatory, GABA1, and GABA2 neuron subtypes with all replicates pooled. Differential expression is defined by FDR < 0.05 and log2FC > 0.25. **e** Sunburst plots of enriched synGO term in excitatory, GABA1, and GABA2 neuron subtypes. **f** Overrepresentation of ASD, SCZ, BD, MDD, and BMI-related genes in excitatory, GABA1, and GABA2 neuron subtypes DEGs. The color of the box shows the odds ratio for enrichment (shades of red for significant enrichment, adjust p < 0.05).